Solid state chemistry of the spin transition polymers $[Fe(Htrz)_3](ClO_4)_2$ and $[Fe(NH_2trz)_3](ClO_4)_2$

by

Eugene Smit

Submitted in partial fulfilment of
the requirements for the degree

Master of Science (Chemistry)

in the

Faculty of Science

University of Pretoria
Pretoria

November 2000

Acknowledgements

The financial support by the University of Pretoria and the National Research Foundation, Pretoria, is gratefully acknowledged.

The following source of the figure used in **Figure 22** is acknowledged:
Inorganic Chemistry, **1997**, 36, 6357-6365. Copyright 1997 American Chemical Society. Special thanks and acknowledgement to Y. Garcia for supplying the figure.

Special thanks and acknowledgement to Doctor Bouchaib Manoun for all his helpful comments and advice.

Finally, a very special thanks and acknowledgement to Professor Danita de Waal, my promoter, for lots of advice and support during this project, but especially for taking me and my project under her wing at a time when it seemed that nobody would.

Ekserp

Spin-oorgang verbindings ondergaan 'n oorgang tussen 'n diamagnetiese lae-spin toestand en 'n paramagnetiese hoë-spin toestand. Hierdie verbindings het moontlike toepassings in optiese skakeling, inligting stoor en –vertoon, sowel as in temperatuur en druk sensors.

Die doelwit van hierdie projek was om inligting te kry oor die strukturuele veranderinge wat plaasvind tydens spin-oorgang in lae-kristallyne, spin-oorgang *polimere*. Infrarooi spektroskopie het getoon dat die Fe-N bindings in die oktaëdriese Fe-N_6 koördinasiesfeer almal verswak tydens die lae-spin na hoë-spin oorgang, maar dat twee van die verbindings tot 'n mindere mate verswak as die ander vier.

Raman spektroskopie het getoon dat 'n moontlike verandering in die koördinasiesfeer simmetrie, tydens die oorgang, daartoe lei dat die Fe-N strekkingsvibrasie onaktief raak. Verder kan die afnemende intensiteit van die Raman band gebruik word om 'n oorgangsfunksie kurwe op te stel.

X-straal poeierdiffraksie het 'n metode uitgelig om die kristallyniteit van die spin-oorgang polimeer $[Fe(Htrz)_3](ClO_4)_2$ te verbeter en uit die analise van die poeier patroon is 'n seloplossing met monokliene simmetrie verkry.

Abstract

Spin-transition compounds exhibit a transition between a diamagnetic low-spin state and a paramagnetic high-spin state. These compounds have potential applications in optical switching, information storage and -display, as well as in temperature and pressure sensors.

This project was aimed at obtaining information on structural changes that occur during spin-transition in poorly crystalline spin-transition *polymers*. Infrared spectroscopy showed that the Fe-N bonds in the octahedral Fe-N_6 coordination sphere all weaken during the low-spin to high-spin transition, with two bonds weakening to a lesser degree than the other four.

Raman spectroscopy showed that a possible change in the coordination sphere symmetry, during transition, leads to the Fe-N stretching vibration becoming inactive and that the decreasing intensity of the Raman band can be used to derive a transition function curve.

X-ray powder diffraction showed a method to increase the crystallinity of the spin-transition polymer $[Fe(Htrz)_3](ClO_4)_2$ and analysis of the powder pattern gave a cell solution with monoclinic symmetry.

Table of Contents

List of Figures

List of Tables

List of Related Achievements

Publications

Infrared Spectroscopy

1. "The Spin-Transition Complexes $[Fe(Htrz)_3](ClO_4)_2$ And $[Fe(NH_2trz)_3](ClO_4)_2$: I. FT-IR Spectra Of A Low Pressure And A Low Temperature Phase Transition", E. Smit, D. De Waal and A. M. Heyns, *Materials Research Bulletin* 35(10), **2000**.
2. "Pressure-dependent FTIR of $[Fe(Htrz)_3](ClO_4)_2$", A. E. Smit, D. De Waal and A. M. Heyns, *Proceedings of the 12th International Conference in Fourier Transform Spectroscopy*, Tokio, Japan, 511-512, **1999**.

Raman Spectroscopy

3. "Low-Frequency Raman Spectra Of The Spin-Transition Complexes $[Fe(NH_2trz)_3](ClO_4)_2$ And $[Fe(Htrz)_3](ClO_4)_2$", E. Smit, B. Manoun and D. De Waal, *Journal of Raman Spectroscopy*, accepted for publication.

X-ray Powder Diffraction

4. "Improvement of X-ray powder diffraction patterns of the spin transition polymer $[Fe(Htrz)_3](ClO_4)_2$", E. Smit, B. Manoun, S. M. C. Verryn and D. de Waal, *Powder Diffraction*, accepted for publication.

Poster Presentations

1. "Pressure-dependent FTIR of $[Fe(Htrz)_3](ClO_4)_2$", A.E. Smit, D. De Waal and A. M. Heyns, *12th International Conference in Fourier Transform Spectroscopy*, Tokio, Japan.
2. "Raman investigation of the low temperature transition of the spin-transition polymer $[Fe(NH_2trz)_3](ClO_4)_2$", E. Smit, B. Manoun and D. De Waal, *SACI 2000, 35th Convention of the South African Chemical Institute*, Potchefstroom, South Africa, 24-29 September 2000.
3. "Improvement of X-ray powder diffraction patterns of the spin-transition polymer $[Fe(Htrz)_3](ClO_4)_2$", E. Smit, B. Manoun, S. M. C. Verryn and D. De Waal, *SACI 2000,*

35th Convention of the South African Chemical Institute, Potchefstroom, South Africa, 24-29 September 2000.

Oral Presentation

1. "Pressure-dependent FTIR of $[Fe(Htrz)_3](ClO_4)_2$", *SACI Young Spectroscopists Symposium*, 1999.

Chapter 1 – General Introduction

"Science and Technology (S and T) are recognised by both developed and developing countries as critical ingredients for socio-economic development. It seems that to survive in modern society all members of the public must possess some understanding of science and technology. As the developed world enters the information age, developing countries, no less the Southern African sub-region cannot remain a perpetual onlooker. The verdict pronounced on any community that does not give due attention to science and technology can be summed up in three words: backwardness, obsolescence and oblivion!"

These strong words, from reference [1], can not, in all fairness, be applied to the academic research departments in South Africa. The Current Reality of SET (Science, Engineering and Technology) in South Africa, as taken from *South Africa's Green Paper on Science and Technology (1996)*[2], shows that our output of scientific publications amounts to 50% of the sub-Saharan total. These however, have shown a slow but steady decline in the past few years, and are mainly concentrated in plant and animal science, geosciences, ecology and environmental science.

We are lagging behind in many high-technology fields that are quickly becoming the basic building blocks of the global village of tomorrow. One obvious example is the field of solid-state electronics i.e. the heart of computers. It is often difficult if not impossible to "reinvent the wheel" when taking financial and/or legislative aspects into consideration, but it seems that we have started to depend on countries like Germany, the USA and Japan to generate most, if not all, of the new technologies that we use. By avoiding such fields of research, we are becoming slaves to the creators of the technologies on which we depend. This kind of attitude is not only detrimental to the growth of SET in our country, but actually limits the progress of all humankind!

In our approach to research, as a developing country, it is important to realise that it is impossible to compete with the creators of today's high technologies. We should rather be predicting what the technologies of tomorrow will be, and start developing them today. Successful technologies are those that solve problems efficiently and many of tomorrow's problems can be deduced by observing current trends. One instance of a current trend, and the problems that arise from this, serves as an example:

The world population is growing at an alarming rate; this is the current trend.

Problems that can easily be deduced from this are shortages of food, housing, employment etc. By identifying such problems, we can start working toward solutions to alleviate, or even eliminate the impact that they will have on tomorrow's society.

There are thousands of observable trends, and millions of possible solutions to the problems related to them. The sensible choice is to identify a foreseeable trend-related problem that will, in the near future, have a marked effect on life in South Africa. This effect can be social, economic, or even environmental. Once such a problem has been identified, possible solutions can be suggested and research can begin.

The whole world, including South Africa, is moving into the Information Age. One of the current trends emanating from the Information Age is a rapid increase in the volume of information. We, along with the rest of the world, are faced with numerous problems in this regard:

- Increased computing power is required to manipulate the information.
- Huge volumes of information must be stored and retrieved fast, accurately, and without omissions.
- Large numbers of computers, that become redundant due to technological demand surpassing their ability, need to be recycled.

New technologies need to be developed to solve some of these problems. Developing new technologies often require new materials that make them possible. One group of materials, which has been identified for application in optical computing, information storage and information display, is *spin-transition polymers*.

In the last forty years the bit length (physical length of one binary digit in passive information storage devices) has decreased from

- 250 μm (the first hard disk from IBM in 1950) to
- 1 μm in audio compact disks and even
- 0.6 μm (through the use of frequency doubling techniques).[3]

To further increase the achievable capacity, there is a crucial need for new materials. Spin-transition polymers offer many interesting capabilities and one of these is very small bit size. The predicted storage density limit for optical writing is **100 bits/μm^2**. Conservative estimates of the potential storage density with spin-transition polymers gives a staggering **22 500 bits/μm^2!** In other words, if an ordinary data compact disk has a capacity of **±600 megabytes**, the spin-transition polymer analogue of similar size will have a capacity of **±132 gigabytes**. Another way of putting it would be to say that one spin-transition polymer disk could contain data that would require approximately 220 compact disks for storage!

It is obvious that spin-transition polymers have the potential to be a very important group of materials in the near future. Since research on spin-transition polymers is still in its infancy, it is possible and in fact imperative that we start research in this field, or face the possibility of once more falling out of the race.

The aim of this research project was

- to *study/review* the existing knowledge on spin-transition;
- to *identify* unknowns or inconclusive theories about spin-transition polymers;

- to *investigate* one or more of these unknowns in order to obtain a better understanding of spin-transition materials in general and polymeric spin-transition compounds in particular, and
- to add to the pool of knowledge on the subject.

From the study/review of spin-transition (Chapter 2) the two spin-transition polymers $[Fe(Htrz)_3](ClO_4)_2$ and $[Fe(NH_2trz)_3](ClO_4)_2$ were identified as good subjects for further investigation. It was determined that more information was needed on the structures of these compounds and on the changes that occur in the structures during spin-transition.

For reasons to be discussed in Chapter 2, three studies were undertaken (Infrared, Raman, and X-ray powder diffraction). The experimental details and special considerations of the three studies are given in Chapter 3. The results obtained from the Infrared, Raman, and X-ray powder diffraction studies are given and discussed in Chapters 4, 5, and 6 respectively.

The conclusions that were drawn from the three studies, together with suggested applications and procedures that could be derived therefrom, are given in Chapter 7.

Chapter 2 – Spin-transition uncovered

2.1 The Spin-Transition Phenomenon

Certain $3d^n$ ($4 \leq n \leq 7$) transition metal compounds, with octahedral ligand-field symmetry, show a transition between a diamagnetic low-spin state and a paramagnetic high-spin state. This is known as spin-transition, also sometimes referred to as spin crossover, magnetic crossover, spin equilibrium or spin isomerism. The transition can be brought about by a change in temperature (ΔT), a change in pressure (ΔP), or by irradiation ($h\nu$). The transition is often accompanied by a pronounced change in the colour of the compound: from purple in the low-spin state to white in the high-spin state. The phenomenon is observed in the solid state as well as in solution.

A substantial amount of research has been done on spin-transition compounds involving Fe^{2+} with the $3d^6$ configuration. In octahedral symmetry the orbital degeneracy is lowered and the 3d metal orbitals are split into the low-lying t_{2g} orbitals and high-lying e_g orbitals (see Figure 1). The double-occupation of the anti-bonding e_g^* orbitals in the high-spin state leads to a weakening (and lengthening) of the Fe-ligand bonds.

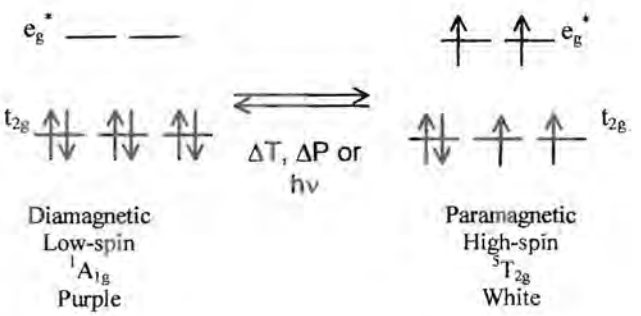

Figure 1 Schematic representation of spin-transition for a $3d^6$ system such as Fe(II)

To a first approximation, the crossover occurs when the enthalpy of the low-spin state is slightly lower than that of the high-spin state. At low temperature, the thermodynamically stable state is the low-spin state. On the other hand, when the temperature is higher than a certain temperature, denoted $T_{½}$, the high-spin state becomes the thermodynamically stable state, because the entropy associated with the high-spin state is much larger than the entropy associated with the low-spin state, and the $T\Delta S$ (temperature multiplied by entropy) gain overcomes the enthalpy loss. $T_{½}$, also known as the critical temperature T_c, is the temperature for which there is coexistence of 50% of low-spin and 50% of high-spin molecules[3].

The transition can be characterised by an x_{HS} = f(Perturbation) curve (see Figure 2), where x_{HS} is the molar fraction of high-spin molecules and the perturbation is temperature- or pressure change or irradiation.

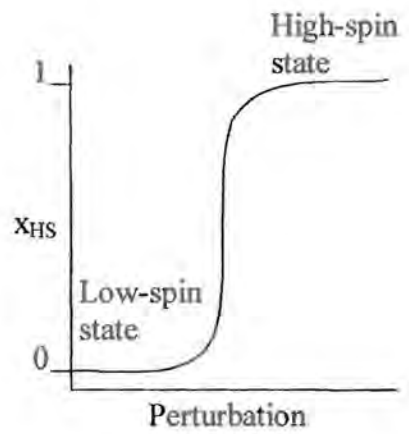

Figure 2 Typical spin-transition function curve

Any technique that gives a response that can be related to x_{HS} as a function of the perturbation can be used to construct such a curve. Techniques that have been used in this regard include: optical observation with UV-vis spectroscopy[4,5], magnetic susceptibility measurements[6-23], Mössbauer spectroscopy[24-38], electron

paramagnetic resonance (EPR) spectroscopy[39,40], single crystal[41-50] and powder[51,52] X-ray diffraction, infrared[53-60] and Raman[61-64] spectroscopy and other techniques including NMR, EXAFS, LAXS[65-67] and heat capacity measurements[68]. Section 2 gives a brief review of the application of these techniques in the study of spin-transition compounds.

2.2 Application of various techniques in the study of spin-transition

2.2.1 Optical Observation (UV-vis or electronic absorption spectroscopy)

According to the ***Tanabe-Sugano (TS)*** diagram for an ion with a d^6 electronic configuration in an octahedral ligand field (see Figure 3), one can expect quite different absorption spectra for high-spin or low-spin complexes[69].

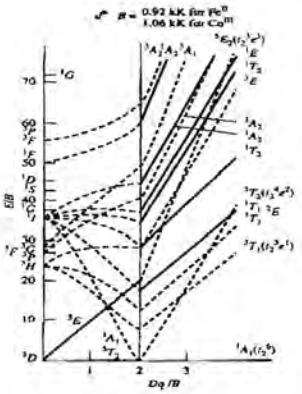

Figure 3 Tanabe-Sugano diagram for an octahedral d^6 complex calculated with the Racah parameters of the free iron(II) ion.

In an Fe^{2+}, d^6, O_h system the purple (low-spin) colour results from the spin-allowed $^1A_{1g} \rightarrow {}^1T_{1g}$ d-d transition occurring at ±520nm. The white (high-spin) colour arises from the fact that the spin-allowed d-d transition of lowest energy in the high-spin state, $^5T_{2g} \rightarrow {}^5E_g$, occurs in the near-infrared (±850nm).

Since the intensity of the 520nm band is proportional to the molar fraction of high-spin molecules, recording the transmittance of the material at 520nm

wavelength, as a function of temperature, gives a transition function curve (see Figure 4).

Optical observation is of particular relevance for Fe(II) compounds in which the d-d bands are not obscured by intraligand or charge-transfer bands.

Electronic absorption spectroscopy can also be used to obtain ligand-field information on the compound.

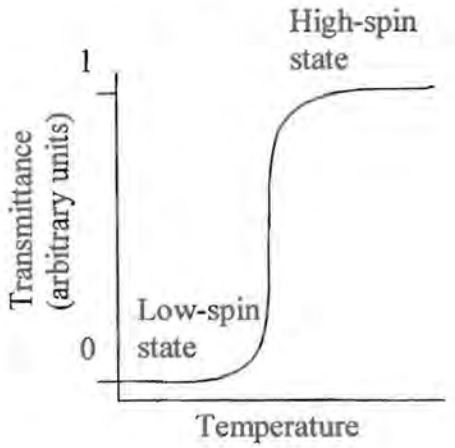

Figure 4 Spin-transition function curve constructed from the recording of the transmittance of the material at 520nm.

2.2.2 Magnetic susceptibility

One of the simplest methods of obtaining a transition function curve consists of measuring the molar magnetic susceptibility (χ_M) as a function of temperature. According to Kahn et al.[70], χ_M obeys the Curie law in the temperature range where all molecules are in the same spin-state, with $(\chi_M T)_{LS}$ and $(\chi_M T)_{HS}$ constant. This is valid if the orbital degeneracy in a strictly octahedral environment is totally removed by symmetry lowering. $x_{HS} = f(T)$ can then be deduced from the experimental $\chi_M T = f(T)$ curve (Figure 5) according to Equation 1. In the case of iron(II) compounds, the low-spin state is diamagnetic and thus $(\chi_M T)_{LS} = 0$ and Equation 1 reduces to Equation 2.

$$x_{HS} = \frac{\chi_M T - (\chi_M T)_{LS}}{(\chi_M T)_{HS} - (\chi_M T)_{LS}} \quad (1)$$

$$x_{HS} = \frac{\chi_M T}{(\chi_M T)_{HS}} \quad (2)$$

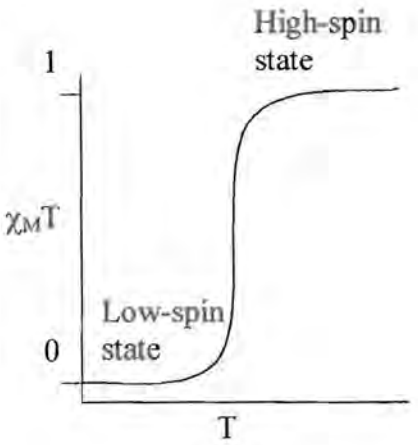

Figure 5 Typical experimental $\chi_M T = f(T)$ curve

2.2.3 Mössbauer spectroscopy

Mössbauer spectroscopy utilises the Mössbauer effect to study the magnetic fields inside ions. Further information on Mössbauer spectroscopy and the use thereof in transition metals chemistry can be found in reference [71]. This technique is especially useful for the study of iron compounds, since the $^{57}_{26}Fe$ nuclide is Mössbauer-active. Distinct signals can, in principle, be obtained when the spin-flipping frequency is lower than the technique frequency scale. Otherwise, a single average signal is obtained. In the case of Fe spin-transition compounds, Mössbauer spectra show two well-resolved quadrupole doublets with variable intensity as a function of temperature. This holds, if the coexisting spin-isomers have lifetimes larger than 10^{-7}s. One of these doublets is associated with low-spin ions and the other with high-spin ions. The high-spin molar fraction can then be deduced from

the relative intensities of these quadrupole doublets.[71] The Mössbauer effect can also provide information on the microscopic environments of the ^{57}Fe nuclei and spin-state interconversion rates but these applications are not discussed here.

2.2.4 Electron Paramagnetic Resonance (EPR; or Electron Spin Resonance, ESR).

EPR is the study of molecules containing unpaired electrons by observing the magnetic fields at which they come into resonance with monochromatic microwave radiation[72]

Distinct low-spin and high-spin EPR-signals are obtained when the spin-state interconversion rate is slower that $\sim 10^{-10} s^{-1}$ (the EPR spectra time scale). If this holds, x_{HS} can be deduced from the relative intensities of the low-spin and high-spin signals. EPR can also provide information on the microscopic environment of the molecular orbitals and on spin-state interconversion rates.

2.2.5 Single crystal and powder X-ray diffraction

As stated in section 1 of this chapter, the excitation of two electrons, from the t_{2g} orbitals to the anti-bonding e_g^* orbitals in Fe(II) complexes, leads to a weakening and lengthening of the Fe-ligand bonds. This change in the metal-ligand bondlength can be observed in crystalline samples with the aid of *single crystal X-ray diffraction.* One example, from reference [4], shows a single crystal diffraction study of the $[Fe_3(4\text{-Ettrz})_6(H_2O)_6]^{3+}$ cation (with 4-Ettrz = 4-Ethyltriazole) at 300K and 105K. The crystal structures are essentially the same, except for a significant shortening of the Fe-N bond in the low-temperature, low-spin state. Metal-ligand bondlengths typically increase by 0.14Å to 0.24Å during the transition from the low-spin state to the high-spin state.[7]

Some spin-transition compounds such as the spin-transition polymers studied here, crystallize poorly. This makes single crystal studies on such compounds difficult, even impossible. In such cases *powder X-ray diffraction* has been used to derive

structural information on spin-transition. In one example[9] the powder diffraction pattern shows broad diffraction peaks for the compound in the low-spin state. Upon heating the sample to the LS→HS transition temperature, a giant enhancement of one of the peaks is observed. This suggests a long-range order along one of the directions in the high-spin state.

2.2.6 Infrared and Raman spectroscopy

Vibrational spectroscopy (i.e. Infrared and Raman) gives information on the vibrational frequencies and force constants of chemical bonds. Since the metal-ligand bondlengths and –strengths of spin-transition compounds change during spin-transition, a lot of useful information can be obtained from their vibrational spectra.

In *infrared spectroscopy*, the metal ligand bands are systematically lower in energy in the high-spin state than in the low-spin state. This is due to the weakening of the metal-ligand bonds in the high-spin state. Other stretching vibrations, which are, for instance, strongly affected by π-backbonding between the metal and the ligand, can also be strongly affected by spin-transition.

Raman spectroscopy, particularly *Resonance Raman*, has been used extensively in the investigation of biological spin-transition systems with iron-porphyrins.
Raman spectroscopy, in combination with infrared spectroscopy, can be used to investigate changes in the symmetry of the compounds during spin-transition.

2.2.7 Other techniques

Proton *Nuclear Magnetic Resonance (NMR)* has been used to study spin-transition. The line widths of Fe(II) complexes are constant in the diamagnetic temperature region but increase markedly in the spin-transition region. At higher temperatures, the line width follows a T^{-1} dependence.[65]

Extended X-ray Absorption fine structure (EXAFS) and *Large angle X-ray scattering (LAXS)* are two other techniques that have been used to obtain structural information from poorly crystalline spin-transition compounds.[66,67] In Chapter 4, reference is specifically made to the results obtained from these studies.

Heat capacity (C_p) measurements have been used to characterise the spin-transition phenomenon and to determine thermodynamic values, such as mixing entropies, of the transition.[24]

2.3 Spin-transition compounds and transition curves

With the possible exception of the cluster compounds HNb_6I_{11} and Nb_6I_{11}, which are also thought to exhibit spin-transition, spin-transition compounds are generally transition metal complexes. These complex materials generically consist of ligands, coordinated to one or more transition metal ions, with non-coordinating counter ions, non-coordinating solvent molecules and, sometimes, non-coordinating water molecules. The compounds can consist of polymeric or singular molecules. In the solid state the different combinations of ligands, metal ions, counter ions and solvents have a marked effect on the long-range cooperative interactions in the material, and therefore lead to differences in the spin-transition behaviour of the material.

Thermally induced spin-transitions in solution are always gradual, because the $x_{HS} = f(T)$ function obeys a simple Boltzmann Law. On the other hand, solid state $x_{HS}(T)$ curves show a much larger variety and can be classified according to the $x_{HS}(T)$ curve shapes. Figure 6 shows schematic representations of the curve shapes of different spin-transition types.[7,24]

- The transition may be smooth, occurring gradually over a large temperature range, similar to spin-transition in solution (Figure 6.**a**).

- The transition may be abrupt, occurring within a few Kelvin (Figure 6.**b**).
- The transition may occur with two discernible steps (gradual or abrupt) and a step or plateau along the $x_{HS}(T)$ curve (Figure 6.**c**).
- The transition may be incomplete at low temperature ($x_{HS} \neq 0$) and/or high-temperature ($x_{HS} \neq 1$), the former situation being observed more often (Figure 6.**d**).
- The transition curves may be strictly identical in the cooling and heating modes or exhibit a hysteresis effect (Figure 6.**e**). In the latter case, the temperature of the LS→HS transition in the heating mode, $T_{½}\uparrow$, is higher than the temperature of the HS→LS transition in the cooling mode, $T_{½}\downarrow$. Both $T_{½}\uparrow$ and $T_{½}\downarrow$ are defined as the temperatures for which the high-spin molar fraction $x_{HS} = 0.5$.

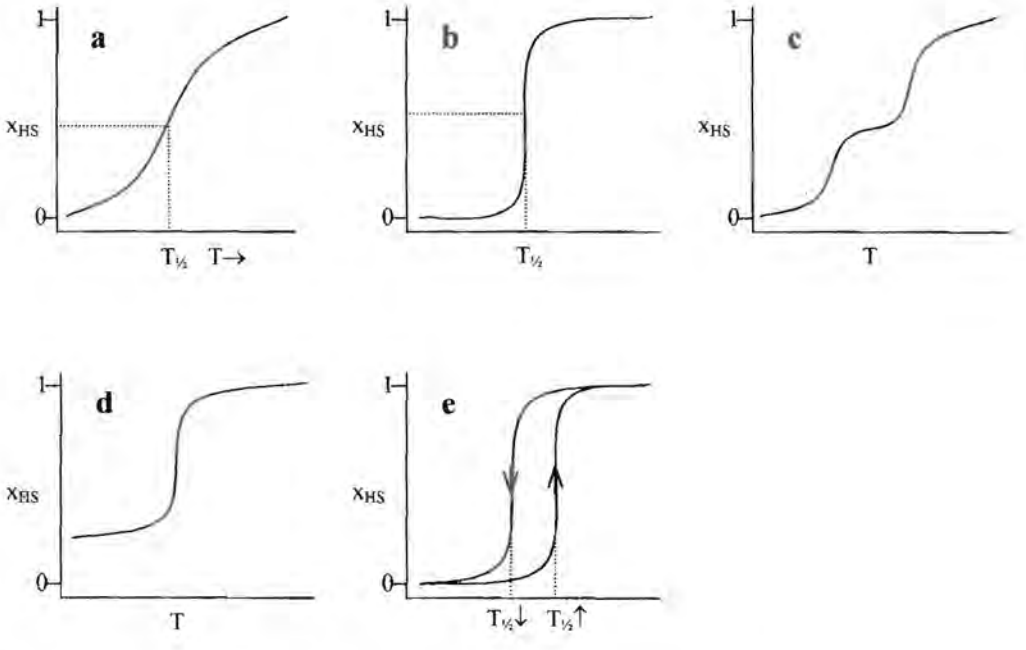

Figure 6 Schematic representations of spin-transition types. $T_{½}$ is defined as the temperature value for which $x_{HS} = 0.5$

2.4 Cooperativity and the effect of chemical and physical factors on the behaviour of spin-transition compounds.

More or less strong long-range molecular interactions in the solid state result in a more or less pronounced cooperative effect. In strongly cooperative transitions, the spin conversion of one molecule induces the transition of the neighbouring molecules through electron-phonon coupling.[73,74] The cooperativity, and thus the behaviour of any spin-transition material, is strongly dependent on the ligand-field strength of coordinating ligands and non-coordinating counter ions. It is also dependent on ion size, ligand size, hydrogen bonding and all other components of the material that affect the electronic and/or vibrational functions within the material. Variation of these factors can lead to changes in $T_{½}$, gradual transitions becoming abrupt, or it can even lead to the suppression of the transition altogether.

The existence of hydrogen bonds generally favours the cooperative character of the transition. A steric hindrance generally has the opposite effect[73]. Exchange of non-coordinating counter anions can lead to an increase in the residual high-spin molecules at low temperatures (see Figure 6.**d**), as well as a complete suppression of the transition[75]. Molecular alloying, a technique where two or more similar ligands are added to the complex in different ratio's, has been used very successfully to alter the critical temperature ($T_{½}$) of transition[6]. Metal dilution, another technique in which the spin-transition–active metal is exchanged for another spin-transition–inactive metal (Mn, Co or Zn), causes the $x_{HS} = f(T)$ curve to become more gradual. Concurrently $T_{½}$ is shifted to lower temperatures[24].

It is generally observed that the preparation technique of spin-transition complexes affects the spin-transition behaviour of the compounds. Crystal defects, as obtained for example by grinding the samples, make the transition less abrupt.[73] When the grain size is smaller, the critical temperatures are lower, the hysteresis loop is less square shaped, and the colour contrast is more, or in some cases less, pronounced.[7]

The lengthening of the metal-ligand bonds in the LS→HS transition cause the spin-transition molecules to be bigger in the high-spin state than in the low-spin state (an observed fact from crystal structure analyses). From this, it can be expected that an increase in pressure will favour the low-spin state. In other words, at elevated pressure the spin transition will occur at higher temperatures than at ambient pressure. High-pressure experiments on iron(II) spin-transition complexes in the solid have always confirmed this.[24]

2.5 Application of spin-transition compounds

The recent appearance, in popular language, of buzzwords such as nanotechnology and micromachines, gives an indication of the increasing scientific and public interest in miniaturisation. Molecular electronics is another term that stems from the miniaturisation trend and refers to molecular-based compounds exhibiting a property, or set of properties, which can be used in devices.[7] Spin-transition compounds have been cited as a potential group of materials for use in molecular electronics. Technological fields where spin-transition may find application include information storage, signal processing, optical switching, optical display, as well as temperature and pressure sensors.

At molecular level, spin-transition corresponds to an intra-ionic electron transfer accompanied by the spin flip of the transferred electrons. The word "intra-ionic" means that the electrons are transferred from the t_{2g} to the e_g orbitals but remain in the immediate environment of the metal ion. There is no electron displacement between sites far apart from each other as it occurs in mixed valence compounds, and no bond displacement as it occurs in photoisomerization. Because of this, the spin-transition compounds do not present any kind of fatigability. The transition may be reproduced as many times as one wants, without altering its characteristics[73]. This gives spin-transition compounds an obvious advantage over competing materials.

Application of a molecular species in information storage or signal processing requires it to have the ability to change electronic ground state as a function of external perturbation. In addition, information storage requires the transition between the two states:

- to present a hysteresis
- to be abrupt
- to have T_c near room temperature
- to be associated with a colour change, and
- to be chemically stable.[7,73]

The chemical stability of spin-transition compounds is generally acceptable and technical preparative methods, such as hermitic encapsulation of granules in resins, lead to even better stability.[3,7]

The requirement of colour change to be associated with the transition is virtually guaranteed for Fe(II) spin-transition compounds since, as stated earlier, the d-d transitions are not obscured by intraligand or charge-transfer bands.

It then remains to define, as accurately as possible, the factors that control the abruptness, hysteresis, and critical temperatures of spin-transition compounds. This has been the object of most recent research on spin-transition. In the previous section, it was shown that abruptness and hysteresis are dependent on the cooperative character in the material. It was shown that increased cooperativity is obtained by use of polymeric spin-transition compounds instead of non-polymeric compounds.

Kröber et al.[6] used the technique of molecular alloying to design a polymeric spin-transition compound with room temperature in the hysteresis loop. The basic

compound is $[Fe(Htrz)_3](ClO_4)_2$, (where Htrz = 1H-1,2,4-Triazole) with the chain structure shown in Figure 7:

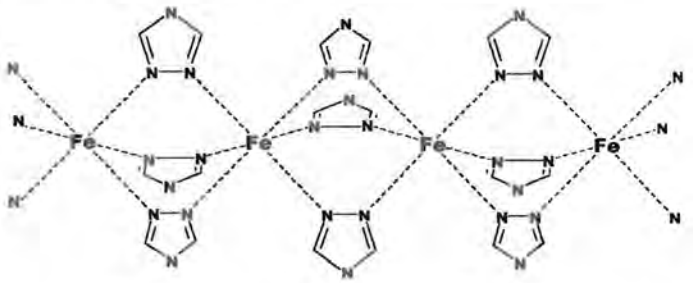

Figure 7 Chain structure of the $[Fe(Htrz)_3]^{2+}$ cation (Hydrogens removed for clarity)

The hysteresis loop of $[Fe(Htrz)_3](ClO_4)_2$ is just above room temperature. $T_c\uparrow$ and $T_c\downarrow$ were shifted to lower temperatures by replacing Htrz with a mixture of Htrz and 4-NH_2trz (where NH_2trz = 4-Amino-1,2,4-Triazole).

Information is stored on magnetic storage media in binary format, i.e. 1's and 0's. A spin-transition material with its hysteresis loop around room temperature ($\therefore T_c\downarrow < T_{Room} < T_c\uparrow$) can be used in a similar way, with the low-spin state symbolising 0 and the high-spin state symbolising 1. If the material is heated to above $T_c\uparrow$, the compound changes to the high-spin state and a 1 is stored. When the compound is cooled to below $T_c\downarrow$, the compound changes to the low-spin state and a 0 is stored. As long is T_{Room} stays between $T_c\downarrow$ and $T_c\uparrow$, the spin state (observed optically or magnetically) gives an indication of the last operation performed on the material and thus a memory effect is obtained. Figure 8 is a diagrammatic representation of this memory effect in spin-transition materials.

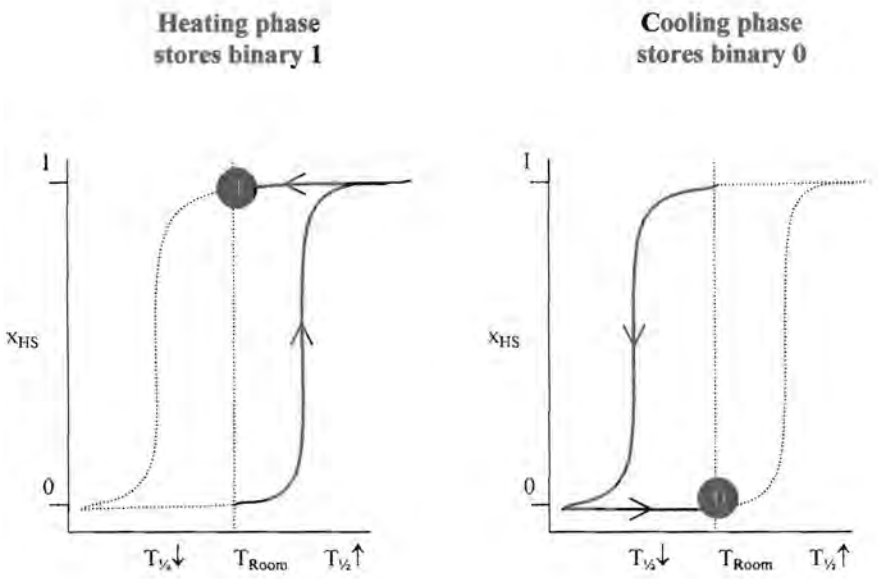

Figure 8 Diagrammatic representation of information storage with spin-transition compounds.

Incorporation of a spin-transition compound into a display device makes it necessary to implement it in a homogeneous layer. This has been performed with screen printing technology. Resistive heating and Peltier element cooling is used for switching the display elements (pixels) between the two states.[7]

Kahn & Martinez[3] have proposed possible application of spin-transition compounds as in situ temperature indicators in magnetic resonance imaging (MRI). Garcia et al.[76] proposed the application of a specific spin-transition compound, which exhibits non-classical spin-transition behaviour, in the simple, accurate detection of a specific temperature.

Zarembowitch & Kahn[73] investigated the possibilities of spin-transition compounds in signal processing, but a lot of work still needs to be done.

2.6 $[Fe(Htrz)_3](ClO_4)_2$ and $[Fe(NH_2trz)_3](ClO_4)_2$ as subjects for further investigation

As stated in Chapter 1, it is imperative that researchers start focussing on new materials that have the potential to become essential parts of tomorrow's high-technologies. By taking into consideration the information discussed above, the two spin-transition polymers $[Fe(Htrz)_3](ClO_4)_2$ and $[Fe(NH_2trz)_3](ClO_4)_2$ (with Htrz = 1H-1,2,4-Triazole and NH_2trz = 4-NH_2-1,2,4-Triazole) were identified for further investigation on the grounds that:

- they exhibit the spin-transition phenomenon (∴ no fatigability)
- they are Fe(II) spin-transition compounds (∴no obscuring intraligand or charge-transfer bands, and thus a colour change from purple to white during the LS→HS transition)
- they are polymeric (∴abrupt transitions and hysteresis), and
- they have been used in molecular alloying to obtain T_c near room temperature.

For these reasons, the two compounds hold great promise for application in molecular electronics.

2.6.1 Available information on $[Fe(Htrz)_3](ClO_4)_2$ and $[Fe(NH_2trz)_3](ClO_4)_2$

The first compound is $[Fe(Htrz)_3](ClO_4)_2$ with Htrz = 1H-1,2,4-Triazole (see Figure 9 of **1H-1,2,4-Triazole**)

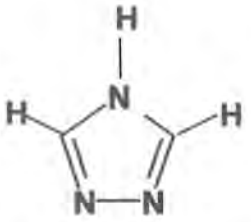

Figure 9 1H-1,2,4-Triazole

Htrz is known to bridge metal ions through the 1,2 or, more exceptionally the 2,4-nitrogen positions[77] leading to polymeric structures, as shown in the Figure 10.

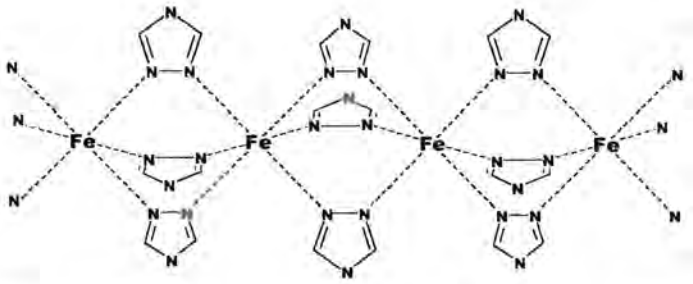

Figure 10 Chain structure of the $[Fe(Htrz)_3]^{2+}$ cation (Hydrogens removed for clarity)

The polymeric structures favour cooperativity. When perfectly dry, the compound shows a smooth spin-transition around 265K with a small thermal hysteresis of ± 5K. With the addition of a small amount of water (1 drop in 50mg $[Fe(Htrz)_3](ClO_4)_2$) the transition becomes very abrupt in both the warming and cooling phase with $T_c\uparrow$= 313K and $T_c\downarrow$= 296K[6]. The addition of water probably causes an increase in the number of hydrogen bonds leading to an increase in the cooperativity (see section 4 above). The transition is accompanied by a purple↔white colour change as discussed in Section 2.1.

The second compound is $[Fe(NH_2trz)_3](ClO_4)_2$ with NH_2trz = 4-NH_2-1,2,4-Triaole. According to Kröber et al[6], the pure material shows a smooth transition around $T_{½}$ = 130K. Note - This value of $T_{½}$ differs from the $T_{½}$ observed by Lavrenova et al[78] and the $T_{½}$ observed in the Raman study presented in Chapter 5 but it is assumed that the difference is caused by differences in sample preparation.

From literature it was also found that $[Fe(Htrz)_3](ClO_4)_2$ and other similar compounds, are generally found to be poorly crystalline powders [9,66,79] and that different batches of the same compound tended to behave very differently as a result of small differences in preparation.[7, 73] It can be assumed that these are the reasons why no Powder Diffraction File (PDF) for $[Fe(Htrz)_3](ClO_4)_2$ could be found in the literature.

No suitable single crystals of these compounds have been obtained. Single crystal X-ray diffraction can therefore not be used to determine the structural changes associated with the spin-transition in these compounds. Other workers have, however, succeeded in characterising similar linear tri-nuclear Fe^{2+} species with 4-substituted-1,2,4-triazole ligands triply bridging the metal ions [14]. According to Kahn and Martinez[3] the structure of Iron(II)-(4-substituted triazole) spin-transition compounds in the low-spin state consists of linear chains in which the neighbouring Fe atoms are triply bridged by the 4-substituted triazole ligands through the N-atoms occupying the 1- and 2-positions **(see** Figure 10 **above).**

The FeN_6 core is close to a regular octahedron. An Fe-Fe-Fe linear path is confirmed by EXAFS and LAXS spectra[66,67] . In the high-spin state, the chain structure is retained but the FeN_6 core is distorted and the peaks characteristic of a three-Fe-atom linear path disappear.

Various infrared studies have shown the effect of spin-transition on the metal-ligand stretching vibrations[53-56,60,80-82] and these can be related to the Fe-N bondlengths.

Lavrenova et al.[78] specifically studied $[Fe(Htrz)_3](ClO_4)_2$ (Htrz = 1H-1,2,4-triazole) and the NH_2trz-analogue (NH_2trz = 4-amino-1,2,4-triazole) using magnetic susceptibility, X-ray powder diffraction, Mössbauer-, diffuse reflectance- and IR-spectrometry but the focus of the study was different from the research presented here.

2.6.2 Conclusions from review of the literature on $[Fe(Htrz)_3](ClO_4)_2$ and $[Fe(NH_2trz)_3](ClO_4)_2$

- More information is required on the structures of $[Fe(Htrz)_3](ClO_4)_2$ and $[Fe(NH_2trz)_3](ClO_4)_2$ and on the structural changes that occur during spin-transition.
- Information is required on the factors that influence the crystallinity of the materials.

2.6.3 Methods selected for investigation

Vibrational spectroscopy (Infrared and Raman) was selected for investigating the structural changes that occur in $[Fe(Htrz)_3](ClO_4)_2$ and $[Fe(NH_2trz)_3](ClO_4)_2$ during spin-transition. These techniques are generally viewed as complimentary, and sometimes alternative, methods to single-crystal X-ray diffraction for obtaining structural information on materials.

Since X-ray powder patterns are critical for phase characterisation and identification, an X-ray powder diffraction study was undertaken. The aim of the study was to overcome the problems of poor crystallinity and batch-to-batch variation mentioned in section 6.1.

Chapter 3 – Experimental and Other Special Considerations

As stated in Chapter 2, the methods selected for the study were Infrared and Raman spectroscopy and X-ray powder diffraction. In this chapter, the experimental details and special considerations of three studies are reported.

3.1 Materials

3.1.1 Syntheses

The two compounds under study were synthesised using the method of Kröber et al.[6]. $[Fe(Htrz)_3](ClO_4)_2$ was prepared by dissolving 2.9g of $Fe(ClO_4)_2.6H_2O$ (Aldrich, USA) in 100ml of a methanol solution containing 0.040g ascorbic acid; 1.656g of 1H-1,2,4-Triazole (Aldrich, USA) was dissolved in 100ml of methanol, and this solution was added to the iron(II) perchlorate / ascorbic acid solution. The mixture was stirred and then quickly roto-evaporated until almost dry. The complex was allowed to air-dry. The other compounds were prepared similarly but with $FeCl_2$ (FlukaChemie) or $FeSO_4.7H_2O$ (Saarchem-Holpro Analitic RSA) instead of the $Fe(ClO_4)_2.6H_2O$ for $[Fe(Htrz)_3]Cl_2$ and $[Fe(Htrz)_3]SO_4$, respectively, and with $4NH_2$-1,2,4-Triazole (Aldrich, USA) instead of the 1H-1,2,4-Triazole for $[Fe(NH_2trz)_3](ClO_4)_2$.

3.1.2 Special Considerations

In the syntheses of the two complexes with $FeCl_2$ and $FeSO_4.7H_2O$, the choice of the Fe(II) salts were made according to availability in the laboratory, without any reference to the literature. According to Haasnoot[83], the use of higher ligand to metal ratios with 4-alkyl substituted triazoles may give low-spin complexes with a FeL_3A_2 composition. Haasnoot expected that such complexes were also chains of triply bridged iron(II) ions. The same assumptions were made for the compounds $[Fe(Htrz)_3]Cl_2$ and $[Fe(Htrz)_3]SO_4$, in this study, but the ligands were Htrz .

3.2 Magnetic Susceptibility Measurements

Magnetic susceptibility measurements were performed using a Gouy-balance with $[Ni(en)_3]S_2O_3$ (en = ethylenediamine) for calibration. A discussion of the process followed for calculating the spin states of all the studied compounds at room temperature, together with the diamagnetic corrections used for the calculation of the unpaired electrons in each complex are given in Annex 1.

3.3 Elemental Analysis of $[Fe(Htrz)_3](ClO_4)_2$

Elemental analysis was performed on the four different samples of $[Fe(Htrz)_3](ClO_4)_2$ that were used in the powder diffraction study. These analyses were performed using a Carlo Erba NA 1500 C/N/S Analyser (with a modification to determine H) for the C, N, and H. The Fe content was determined with ICP-OE. The results from these analyses are given in Annex 2 together with the theoretical mass percentages of two possible forms of the compound.

3.4 Infrared Spectra

3.4.1 Sample Preparation

The mid-infrared spectra (4000 - 400 cm^{-1}) and far-infrared spectra (650 - 50 cm^{-1}) were recorded using a Bruker IFS 113v FT-IR spectrometer. Samples were recorded as KBr pellets in the mid-infrared and polyethylene pellets in the far-infrared. To avoid the influence of an externally applied pressure, the far-infrared spectra of the low-pressure phase transition in $[Fe(Htrz)_3](ClO_4)_2$ were obtained by preparing an ordinary polyethylene pellet and dripping the complex, suspended in methanol, onto the pellet. The sample was allowed to dry in air, leaving only the $[Fe(Htrz)_3](ClO_4)_2$ complex on the surface. Therefore, the $[Fe(Htrz)_3](ClO_4)_2$ complex was not mixed with the polyethylene and subjected to pressure when the pellet was prepared. Low pressures were obtained in the evacuated sample chamber of the infrared instrument. The high-temperature far-infrared spectra of $[Fe(Htrz)_3](ClO_4)_2$ were obtained by heating the sample pellet and metal pellet holder to 353K in a furnace and recording

the spectrum before the sample could cool to below 323K. The low-temperature far-infrared spectra of $[Fe(NH_2trz)_3](ClO_4)_2$ were recorded using a liquid nitrogen cryostat to maintain the temperature of the sample.

3.5 Raman Spectra

3.5.1 General Considerations

Given the structural complexity of the studied systems, (i.e. the presence of multiple organic ligands, triply bridging between two metal centres at a time, forming chains of unknown length) complete assignment of their solid state Raman spectra would seem very difficult. The interest in this Raman study was mainly focused on the structural changes that occur in the Fe-N_6 coordination sphere during spin-transition, and therefore no special interest was paid to the internal modes of the NH_2trz and Htrz rings. Literature data on 1H-1,2,4-Triazole[84,85], and the ClO_4^- and SO_4^{2-} anions[86] were, however, useful in recognition of the X-Triazole (X = H, NH_2) and the anion modes, which were not expected to suffer major changes upon complexation.
Since XH (X = C, N) stretching bands (expected to dominate above 1800 cm^{-1}), ring stretching and deformations (expected in the 1800-1100 cm^{-1} region) and CH deformations (found below 1100 cm^{-1}) were not of interest, the spectra discussed here were recorded in the low-wavenumber region (650-50 cm^{-1}), where lattice modes and metal-ligand stretchings could be expected.

3.5.2 Sample Preparation and Instrumental Parameters

The Raman spectra of the powdered samples were recorded using the 10X objective of the Dilor XY Raman microprobe with a spectral resolution of 2 cm^{-1}. The samples were excited using the 514nm line of an argon-ion laser (Coherent Model Innova 300) with a laser output power of 100mW and an integration time of 60s. The low-temperature spectra were recorded with the aid of a Linkum TMS93 liquid nitrogen cryostat, fitted with an HFS91 stage and LNP cooling pump.

3.6 X-ray Powder Diffraction

3.6.1 General Considerations

For the purpose of the powder diffraction study presented here, four different sample batches of $[Fe(Htrz)_3](ClO_4)_2$ were prepared using the method described above. The ages of the different samples at the time of the investigation, are given in Table 1.

Table 1 Ages of the four different $[Fe(Htrz)_3](ClO_4)_2$ samples at the time of investigation.

Sample Name	Sample Age
Sample 1	1 day
Sample 2	1 week
Sample 3	15 months
Sample 4	2 hours

At the end of the syntheses, the complex, a white paste on the walls of the flask, was scraped onto a watch glass to air-dry. It turned purple upon cooling to room temperature. The soft paste quickly dried to form a very hard solid. It is assumed that this quick drying/setting behaviour probably retards further evaporation of the solvent from the product. The older samples (2 and 3) were stored in closed bottles, from directly after synthesis, in the form of the hard solid mentioned above. Any further evaporation of the solvent from the samples was considered negligible.

The elemental analyses of the samples (Annex 2) showed that the proper formula for the compound is $[Fe(Htrz)_3](ClO_4)_2 \cdot 1.85H_2O$. This formula is only used in the discussion of the X-ray powder diffraction study, since the degree of hydration of the compound was not of particular importance in the infrared and Raman studies.

3.6.2 Sample Preparation and Instrumental Parameters

All samples were ground by hand in an agate mortar and specimens were left in open air to dry at room temperature when required.

The XRD analyses were performed on a Siemens D-501 automated diffractometer. Instrumental conditions are summarised in Annex 3. The various ranges of 2θ, step sizes, measuring times and internal d-spacing standards (where applicable) are given together with the relevant patterns.

Chapter 4 – Infrared Study: Results and Discussion

In this chapter the results of the infrared study of $[Fe(Htrz)_3](ClO_4)_2$ and $[Fe(NH_2trz)_3](ClO_4)_2$, are reported and discussed.

4.1 Mid-infrared

4.1.1 Assignment of the bands

The room temperature mid-infrared spectra of $[Fe(Htrz)_3](ClO_4)_2$, $[Fe(NH_2trz)_3](ClO_4)_2$, $[Fe(Htrz)_3]SO_4$ and $[Fe(Htrz)_3]Cl_2$ are shown in Figure 11.

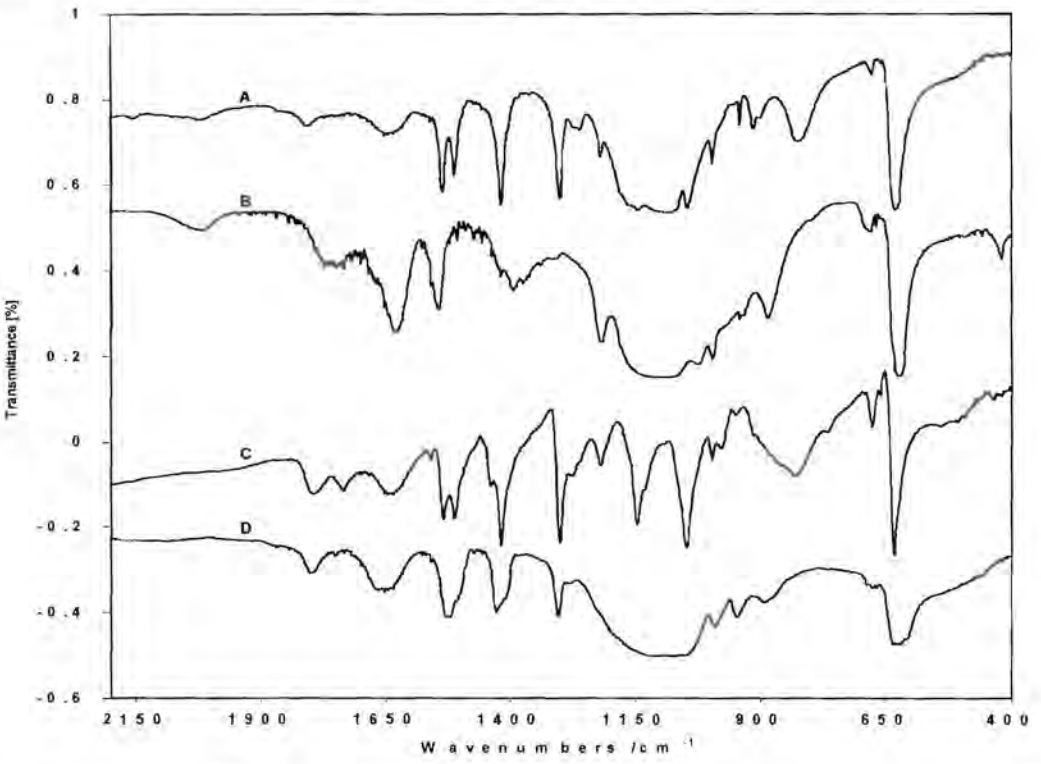

Figure 11 Mid-infrared spectra of (from top to bottom): A. $[Fe(Htrz)_3](ClO_4)_2$, B. $[Fe(NH_2trz)_3](ClO_4)_2$, C. $[Fe(Htrz)_3]Cl_2$, and D. $[Fe(Htrz)_3]SO_4$.

Annex 4 Table I compares the mid-infrared spectra of $[Fe(Htrz)_3](ClO_4)_2$, $[Fe(Htrz)_3]Cl_2$ and the free ligand 1,2,4-Triazole. This shows that the bands observed for the complexes are mainly due to vibrations of the ligand, slightly perturbed by coordination. This observation has been made before for similar compounds such as $[Fe(bipy)_3]^{2+}$, $[Ni(phen)_3]^{2+}$ and $[Zn(phen)_3]^{2+}$ (where bipy = 2,2'-bipyridine and

phen = 1,10-phenanthroline)[87]. The infrared vapour-phase fundamentals for the free 1,2,4-Triazole have been assigned by Bougeard et al.[84], who stated that the fundamental frequencies show no great differences for the gas and solid phases.
The ClO_4 -anion has characteristic vibrational frequencies at 935 cm^{-1} (medium), 460 cm^{-1} (very weak), 1050-1170 cm^{-1}(broad strong) and 630 cm^{-1}(strong). These peaks obscure the Htrz-peaks in the mid-infrared spectrum of the complex, hence the spectrum of the $[Fe(Htrz)_3]Cl_2$ complex was used to eliminate the interfering ClO_4-peaks.

4.1.2 1,2-Bicoordination of the ligands

According to Haasnoot et al.[88] the absence or strongly reduced intensity of the first ring torsion (R_8 in Annex 4 Table 1) of Htrz, indicates C_{2v} symmetry and 1,2-coordination of the ligand. A band around 1215 cm^{-1} is always found in 1,2-bi-coordinating triazole and, in all bidentate triazole spectra, the CH-bending vibration is found around 1305 cm^{-1}. Careful inspection of the recorded mid-infrared spectra shows the absence or strong reduction of the R_8 ring torsion in all four compounds. The other vibrations that are indicative of 1,2-bicoordination can also be seen in the spectra of compounds $[Fe(Htrz)_3](ClO_4)_2$, $[Fe(Htrz)_3]Cl_2$ and $[Fe(Htrz)_3]SO_4$. This leads to the conclusion that $[Fe(Htrz)_3]Cl_2$ and $[Fe(Htrz)_3]SO_4$ indeed contain the bidentate ligand in a bridging coordination and could therefore have the same chain structure as $[Fe(Htrz)_3](ClO_4)_2$. The R_9 ring torsion vibrations of $[Fe(Htrz)_3]Cl_2$ and $[Fe(Htrz)_3]SO_4$ split into more than one overlapping band. This would indicate an inequivalence of the coordinated bridging ligand molecules, as has been observed for similar compounds [89].

It is important to note that the mid-infrared spectra of $[Fe(Htrz)_3](ClO_4)_2$ and $[Fe(NH_2trz)_3](ClO_4)_2$ also contain strong peaks near 635 cm^{-1}. These are assigned to a combination of the out-of-plane vibration of the ligands and a strong ClO_4-band that occurs at 630 cm^{-1} (see Figure 11).

4.1.3 Hydration-dehydration during spin-transition

A broad band at 3500 cm^{-1} in the low temperature (low-spin) mid-infrared spectrum of $[Fe(Htrz)_3](ClO_4)_2$ disappears upon heating the sample to above T_c (323 K). This peak reappears with the same intensity upon cooling to room temperature. It is possible that this band represents OH stretching vibrations of adsorbed water and could then indicate that dehydration occurs during the low-spin to high-spin transition and that re-hydration occurs during the high-spin to low-spin transition. The possibility of dehydration / re-hydration during the low-spin to high-spin transition would not be surprising as it has been observed in other spin transition compounds [79]. The influence of water of crystallisation on the spin transition of $[Fe(Htrz)_3](ClO_4)_2$ was also studied by Lavrenova et al [78]. According to the authors the compound $[Fe(Htrz)_3](ClO_4)_2.H_2O$, which is low-spin at room temperature, is converted to a high-spin compound upon the loss of water. The possibility of hydration-dehydration was not investigated here in detail.

4.1.4 Mid-infrared of $[Fe(NH_2trz)_3](ClO_4)_2$

The mid-infrared spectrum of $[Fe(NH_2trz)_3](ClO_4)_2$ contains, as was the case for $[Fe(Htrz)_3](ClO_4)_2$ and $[Fe(Htrz)_3]Cl_2$, mainly the vibrations of the ligand, slightly perturbed by coordination. Strong peaks of the ClO_4-counter anion again obscure the same regions.

4.2 Far-infrared

4.2.1 Pressure dependence of the spin state of $[Fe(Htrz)_3](ClO_4)_2$

The changes in the far-infrared spectrum of $[Fe(Htrz)_3](ClO_4)_2$ at pressures between 200mbar and 110mbar are shown in Figure 12. Various studies have been performed on spin-transition compounds where the high-spin to low-spin transition is brought about under high pressures[18,37,58,90,91,92]. In these studies, various problems related to high-pressure experiments e.g. shear stress and gasket related difficulties, were usually experienced.

Here the far-infrared spectra show that, in the opposite direction, the low-spin to high-spin transition in $[Fe(Htrz)_3](ClO_4)_2$ is also brought about by *lowering* the pressure on the sample to 110mbar. In iron(II) spin-transition compounds the Fe-ligand stretching vibration frequency shifts towards lower wavenumbers from around 400 cm^{-1} in the low-spin state to around 250 cm^{-1} in the high-spin state. This is also observed here for $[Fe(Htrz)_3](ClO_4)_2$ with the Fe-N stretching frequency at 299 cm^{-1} in the low-spin state and at 263 cm^{-1} in the high-spin state. This decrease in frequency results from the double occupation of the anti-bonding e_g orbitals of the d^6 Fe(II) in the high-spin state, leading to the weakening (and lengthening) of the Fe-N bonds.

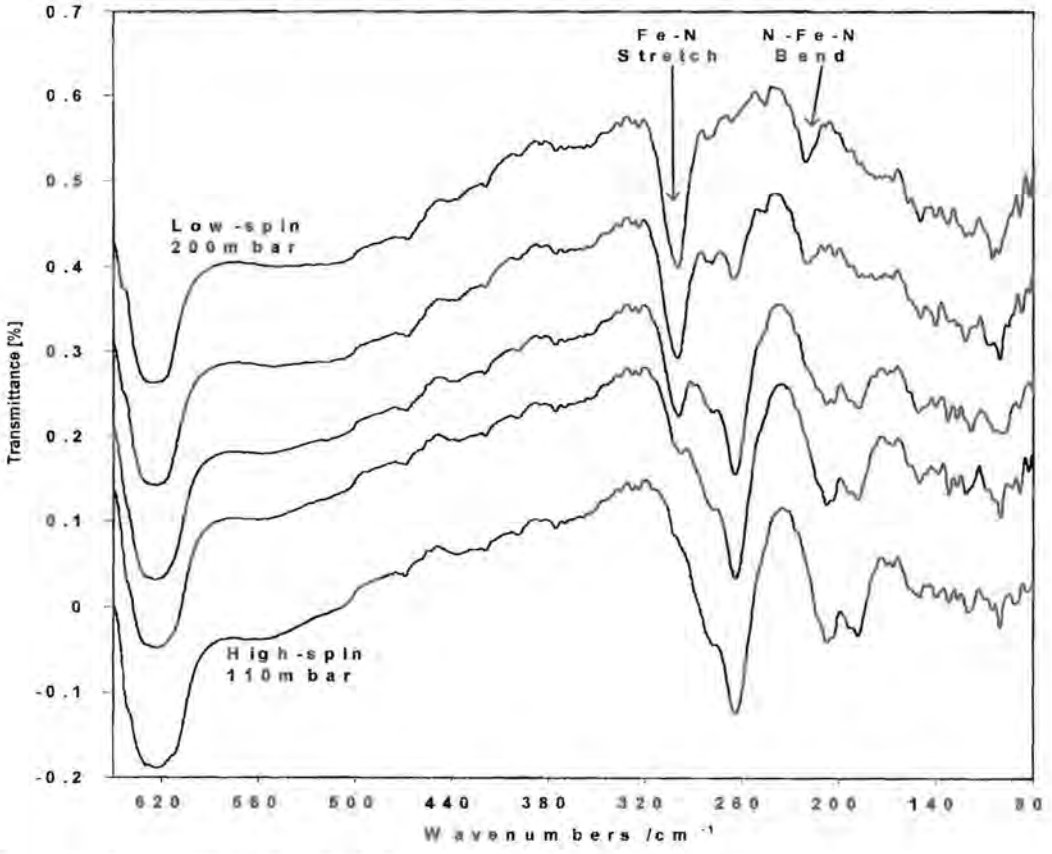

Figure 12 Pressure dependent far-infrared spectra of $[Fe(Htrz)_3](ClO_4)_2$

Faniran and Bertie[85] predicted and assigned all 15 infrared-active lattice modes for the free Htrz-ligand. All 15 frequencies are at wavenumbers below 200 cm^{-1}, thus the

two peaks at 299 cm^{-1} and 221 cm^{-1} in the far-infrared spectrum of the low-spin state of $[Fe(Htrz)_3](ClO_4)_2$ can be assigned to the Fe-N stretching and N-Fe-N bending modes, respectively. Similar assignments have been made for $[Fe(bipy)_2](ClO_4)_2$ (bipy = 2,2'-bipyridine) by Hutchinson et al.[82].

In the high-spin state the Fe-N stretching vibrations move towards lower wavenumbers, viz. 263 cm^{-1} for the stretching mode, with a overlapping band appearing at 280 cm^{-1}, and 214 - 204 cm^{-1} for the N-Fe-N bending vibration. The latter band consists of at least three overlapping bands in the high-spin state.

The low-pressure spin-transition was observed here for the first time in the evacuated sample chamber of the FT-IR instrument. At 200mbar and 298 K the spectrum of the low-spin, purple state is obtained. At 110mbar and 298 K the spectrum of the high-spin white coloured state is obtained. The transition was confirmed by comparing the infrared spectrum of the low-pressure state with that of the high-spin state of the same compound obtained at high temperatures. The infrared spectrum of the high-temperature (T > 323K), white coloured state (i.e. confirmed high-spin state) of $[Fe(Htrz)_3](ClO_4)_2$ was recorded at 200mbar and 330 K. The spectrum corresponds to the one recorded of the low-pressure (110mbar), room temperature $[Fe(Htrz)_3](ClO_4)_2$. The low-pressure transition can also be observed visually by placing a sample of the low-spin, purple $[Fe(Htrz)_3](ClO_4)_2$ in a glass bottle and evacuating the bottle to 110mbar. As can be expected for a low-spin to high-spin transition, the sample changes colour from purple to white. Since the pressure change is very small compared to other pressure induced spin transitions, it is possible that the transition mechanism also includes some degree of hydration / de-hydration. This supposition is supported by the apparent de-hydration / hydration observed in the mid-infrared spectra (see above).

4.2.2 Far-infrared of $[Fe(NH_2trz)_3](ClO_4)_2$

The far-infrared spectra of $[Fe(NH_2trz)_3](ClO_4)_2$ in the temperature range 82 - 298 K are shown in Figure 13. The strong band at 250 cm^{-1} in the room temperature high-spin state is the Fe-N stretching vibration. It seems to consist of two overlapping bands at 254 cm^{-1} and 247 cm^{-1}. The intensity of these bands decreases steadily with decreasing temperature.

4.2.3 Far-infrared of $[Fe(Htrz)_3]Cl_2$ and $[Fe(Htrz)_3]SO_4$

The far-infrared spectra of $[Fe(Htrz)_3]Cl_2$ and $[Fe(Htrz)_3]SO_4$ are compared in **Figure 14**. $[Fe(Htrz)_3]SO_4$ has a strong, broad band at 249 cm^{-1}, which represents the Fe-N stretching vibration of a high-spin $[Fe(Htrz)_3]^{2+}$- complex. This band in $[Fe(Htrz)_3]SO_4$ is composed of two overlapping bands at 270 cm^{-1} and 249 cm^{-1}.

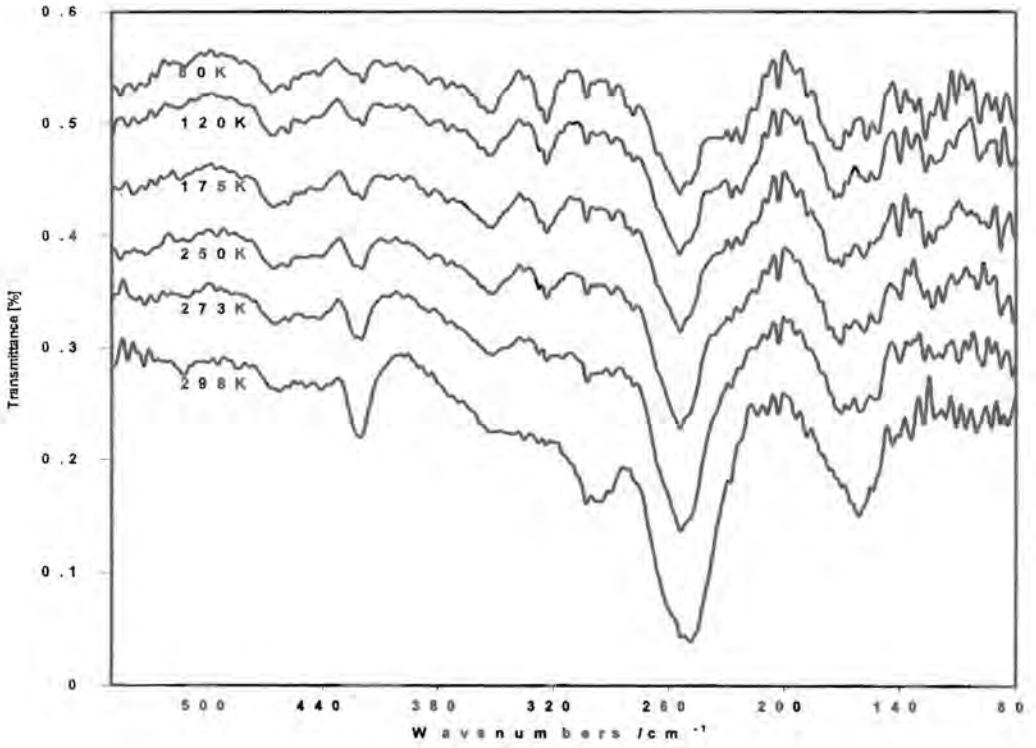

Figure 13 Temperature dependent far-infrared spectra of $[Fe(NH_2trz)_3](ClO_4)_2$.

4.2.4 Changes in Fe-N bond lengths during spin-transition

The information obtained from the far-infrared spectra can be summarised as follows:

In the low-spin state spectra of $[Fe(Htrz)_3](ClO_4)_2$ and $[Fe(Htrz)_3]Cl_2$ a single band is observed for the Fe-N stretching vibration around 300 cm^{-1}. A single band is observed for the N-Fe-N bending vibration in $[Fe(Htrz)_3](ClO_4)_2$ around 220 cm^{-1}. This corresponds to the view of a regular octahedral coordination sphere with six equivalent Fe-N bonds.

For the high-spin state of $[Fe(Htrz)_3](ClO_4)_2$, $[Fe(NH_2trz)_3](ClO_4)_2$ and $[Fe(Htrz)_3]SO_4$ the Fe-N stretching frequency decreases to around 250 cm^{-1} and consists of at least two overlapping bands (280, 263 cm^{-1} for $[Fe(Htrz)_3](ClO_4)_2$ and 279, 247 cm^{-1} for $[Fe(Htrz)_3]SO_4$. This suggests that there are two different types of Fe-N bonds in the high-spin state.

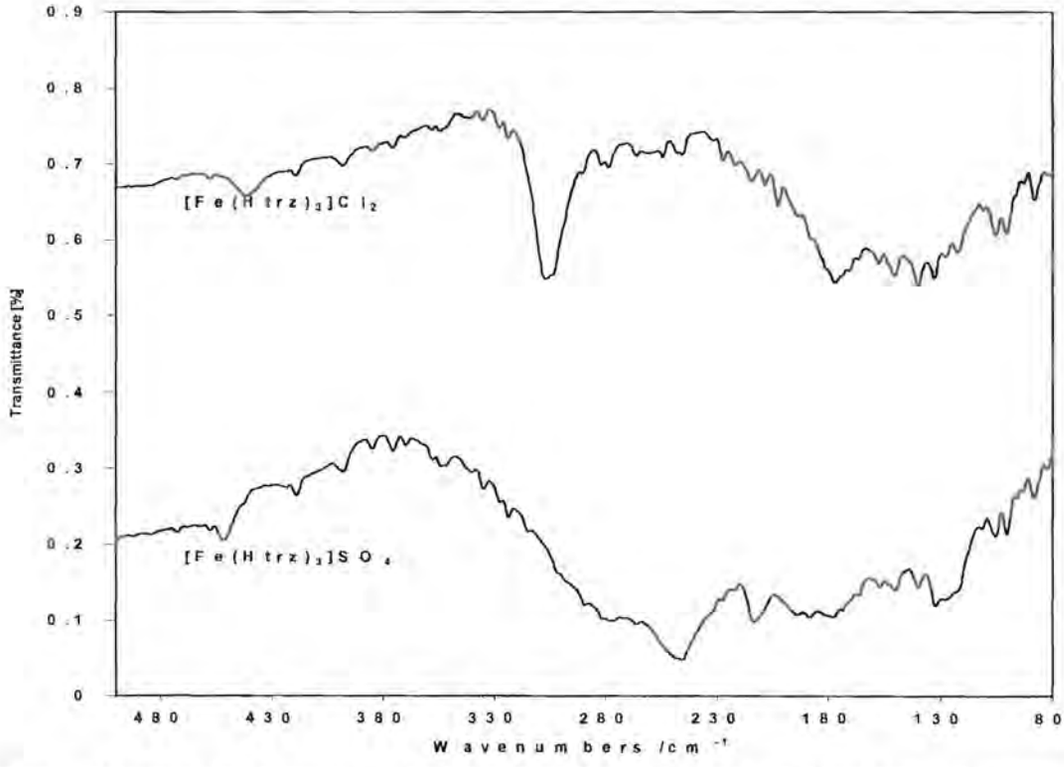

Figure 14 Comparison between the far-infrared spectra of low-spin $[Fe(Htrz)_3]Cl_2$ and high-spin $[Fe(Htrz)_3]SO_4$.

The results would indicate that, in going from the LS to the HS state, all six Fe-N bonds in the coordination sphere are weakened, but two of the bonds (eg. along the z-axis) are weakened to a lesser degree than the other four. This would explain the doubly degenerate Fe-N bands in the high-spin infrared spectra and the distortion of the octahedral arrangement as discussed by Kahn and Martinez[3]. The symmetry of the coordination sphere would thus change from O_h to D_{4h}. It can also be expected that two types of Fe-N bonds in the coordination sphere will result in three types of N-Fe-N bending vibrations (strong-strong, strong-weak, and weak-weak). This would therefore explain the splitting of the N-Fe-N bending vibration of $[Fe(Htrz)_3](ClO_4)_2$ into multiple bands.

Chapter 5 – Raman Study: Results and Discussion

In this Chapter the results of the Raman study of $[Fe(NH_2trz)_3](ClO_4)_2$ and $[Fe(Htrz)_3](ClO_4)_2$, are reported and discussed.

5.1 Composition of the Raman spectrum of $[Fe(NH_2trz)_3](ClO_4)_2$

$[Fe(NH_2trz)_3](ClO_4)_2$ occurs in the high-spin state at room temperature[6]. Figure 15 shows the Raman spectrum of the high-spin state of $[Fe(NH_2trz)_3](ClO_4)_2$ at room temperature. In this spectrum, the various bands can be assigned as follows: all bands below 200 cm^{-1} are NH_2trz lattice modes and the bands at 458 cm^{-1} and 625 cm^{-1} are respectively assigned to the $\nu_2(E)$ and $\nu_4(F_2)$ modes of the non-coordinated ClO_4-anion[86]. These assignments compare very well with the spectra of the pure constituent compounds, $4NH_2$-1,2,4-Triazole and $Fe(ClO_4)_2$, and support the assumption that the lattice and anion modes do not suffer major changes during complexation. The tentative assignment of the NH_2trz and Htrz bands, together with those of the relevant anions in the studied complexes, are presented in Table I and Table II of Annex 5, respectively.

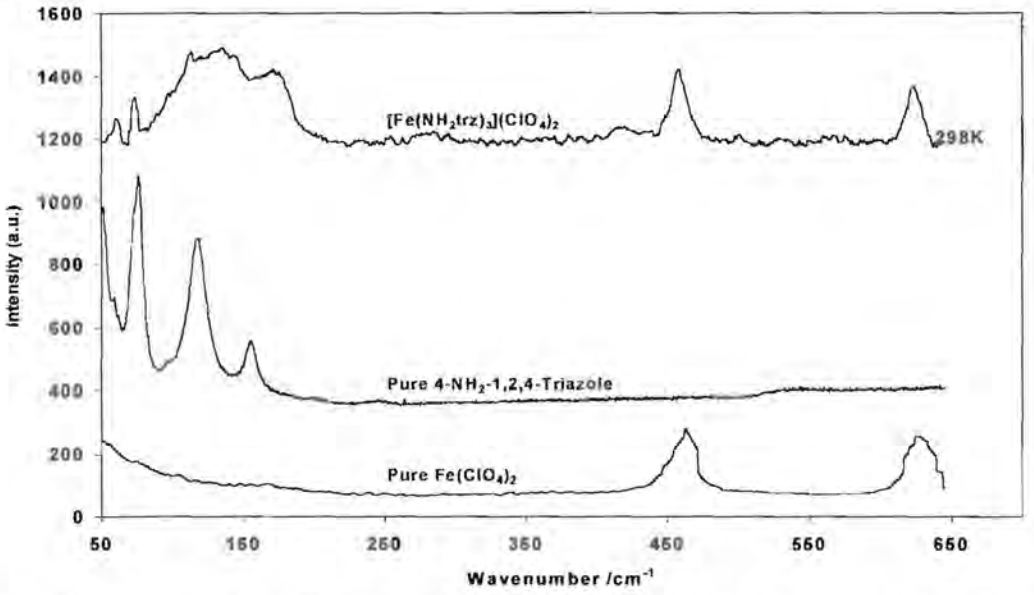

Figure 15 Comparison of the Raman spectra of $[Fe(NH_2trz)_3](ClO_4)_2$ with its pure starting materials, 4-NH_2-1,2,4-Triazole and $Fe(ClO_4)_2 \cdot 6H_2O$. (Note – The recorded spectrum of $[Fe(NH_2trz)_3](ClO_4)_2$ was of very low intensity and has been amplified for comparison).

5.2 Temperature dependence of the $[Fe(NH_2trz)_3](ClO_4)_2$ Raman spectrum

Upon lowering the temperature of the $[Fe(NH_2trz)_3](ClO_4)_2$ sample (Figure 16), the bands associated with the lattice modes grow increasingly resolved, as can be expected, however, a new band appears at 244 cm^{-1}.

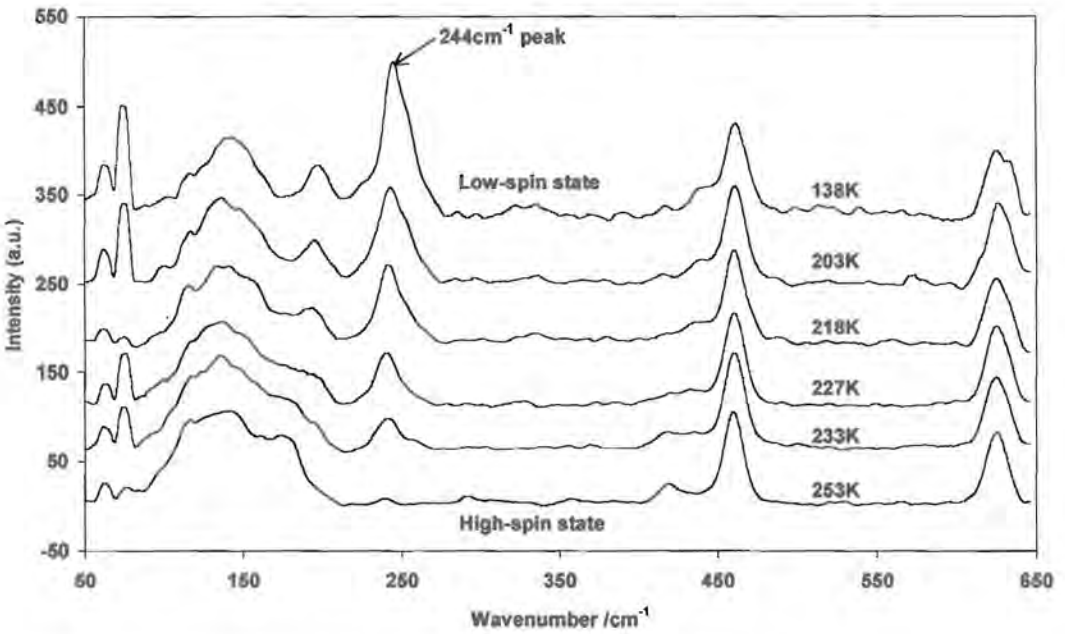

Figure 16 Temperature dependent Raman spectra of $[Fe(NH_2trz)_3](ClO_4)_2$

5.3 Comparison of the Raman spectra of $[Fe(NH_2trz)_3](ClO_4)_2$ with those of $[Fe(Htrz)_3](ClO_4)_2$, $[Fe(Htrz)_3]Cl_2$ and $[Fe(Htrz)_3]SO_4$

Comparison of the spectra of all four investigated compounds in their various spin-states (Figure 16 and Figure 17), reveals an interesting trend: Figure 17 shows the spectra of the high-spin compound $[Fe(Htrz)_3]SO_4$ (Figure 17 – bottom) and the low-spin compound $[Fe(Htrz)_3]Cl_2$ (Figure 17 – top). Note that the high-spin $[Fe(Htrz)_3]SO_4$ spectrum only contains the lattice modes below 200 cm^{-1} and the E and F_2 modes of the SO_4^{2-} anion[86], whilst the low-spin $[Fe(Htrz)_3]Cl_2$ spectrum has another band at 281 cm^{-1} in addition to the lattice modes. Furthermore, if the

high-spin spectrum of $[Fe(Htrz)_3](ClO_4)_2$ (Figure 17 – 2nd from bottom) is compared to its low-spin spectrum* (Figure 17 – 2nd from top), and it can be seen that the low-spin spectrum contains an extra band at 283 cm^{-1}. (*Note: Although $[Fe(Htrz)_3](ClO_4)_2$ normally occurs in the low-spin state at room temperature, the sample had to be cooled to 123K for recording of the low-spin state Raman spectrum. This was done in order to prevent local heating, by the excitation laser, from thermally inducing the low-spin to high-spin transition, which is why the high-spin state Raman spectrum can be obtained at 298K).

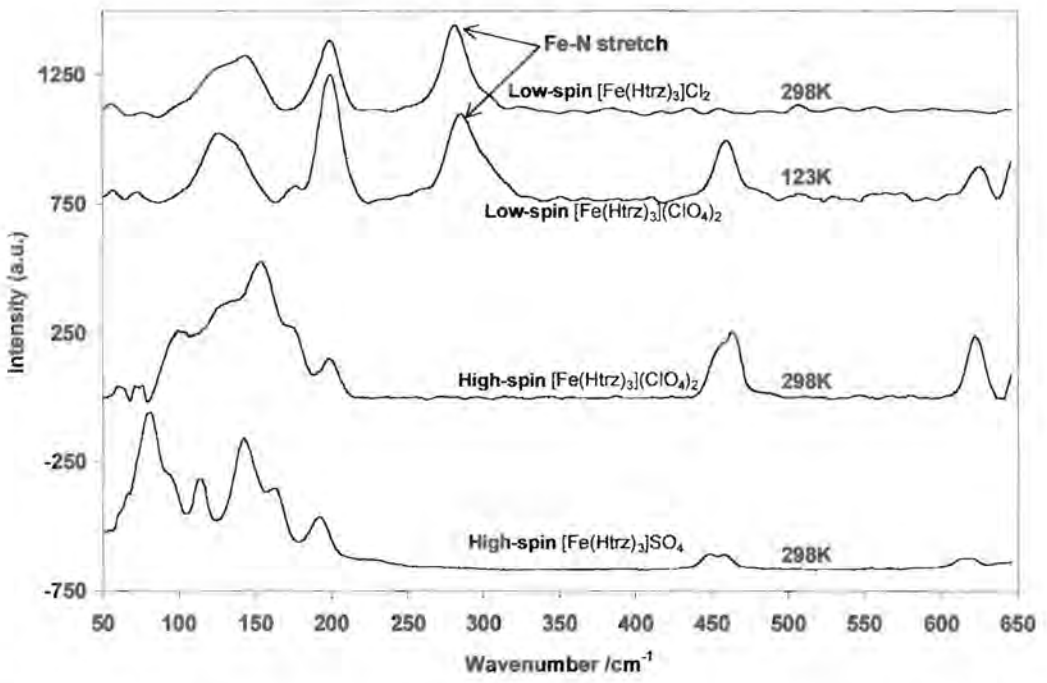

Figure 17 Raman spectra of low-spin $[Fe(Htrz)_3]Cl_2$, low-spin $[Fe(Htrz)_3](ClO_4)_2$, high-spin $[Fe(Htrz)_3](ClO_4)_2$ and high-spin $[Fe(Htrz)_3]SO_4$.

In summary, the spectra of all the investigated compounds in the low-spin state show a band in the region 200-300 cm^{-1}, which does not appear in the high-spin state.

The infrared study of these compounds (Chapter 4) showed that the Fe-N stretching vibration in the infrared spectra can be found at 299 cm^{-1} for $[Fe(Htrz)_3](ClO_4)_2$ in the low-spin state, at 300 cm^{-1} for $[Fe(Htrz)_3]Cl_2$ in the low-spin state, and at 250 cm^{-1} for $[Fe(NH_2trz)_3](ClO_4)_2$ in the low-spin state. It is therefore reasonable to expect the Fe-N stretching vibration in the 200-300 cm^{-1} region of the Raman spectrum, possibly with the Fe-N stretching frequency of $[Fe(NH_2trz)_3](ClO_4)_2$ lower than that of $[Fe(Htrz)_3](ClO_4)_2$ and $[Fe(Htrz)_3]Cl_2$.

5.4 Assignment of the Fe-N band

From the discussion above, it is proposed that the band that appears in the 200-300 cm^{-1} region of the Raman spectra of the low-spin compounds presented here, is the Fe-N stretching mode. This assignment is furthermore supported by a similar assignment of a 220-224cm^{-1} iron-histidine Resonance Raman stretching vibration in deoxyhemoglobins from insect larvae[93].

5.5 Obtaining the spin-transition function curve

Yet another supporting argument for the assignment of the new band to the Fe-N stretching vibration is as follows: The low-temperature induced spin-transition of $[Fe(NH_2trz)_3](ClO_4)_2$ was observed by Lavrenova et al.[78] using magnetic susceptibility measurements. These authors constructed a transition curve by plotting μ_{eff} against temperature. The spin-state of the compound changes gradually from high-spin to low-spin upon cooling to below 210K. By normalising the spectral intensities of the $[Fe(NH_2trz)_3](ClO_4)_2$ Raman spectra investigated here, with respect to the ClO_4-band at 464cm^{-1}, and then plotting the integrated areas under the 244cm^{-1} peaks vs. temperature, a curve is obtained (Figure 18). This curve closely resembles the μ_{eff} vs. temperature transition curve of Lavrenova et al.[78]. Since it is known that the Fe-N bond lengths change during spin-transition[3,6], a change in the Fe-N stretching band can be expected and therefore the similarity to the μ_{eff} vs. temperature curve is probably not a coincidence.

The absence of a comparable Fe-N stretching band in the high-spin spectra of the investigated compounds remains unexplained. It could be suggested that changes in the Fe site symmetry, that occur during the transition from the high-spin state to the low-spin state, lead to the band becoming inactive.

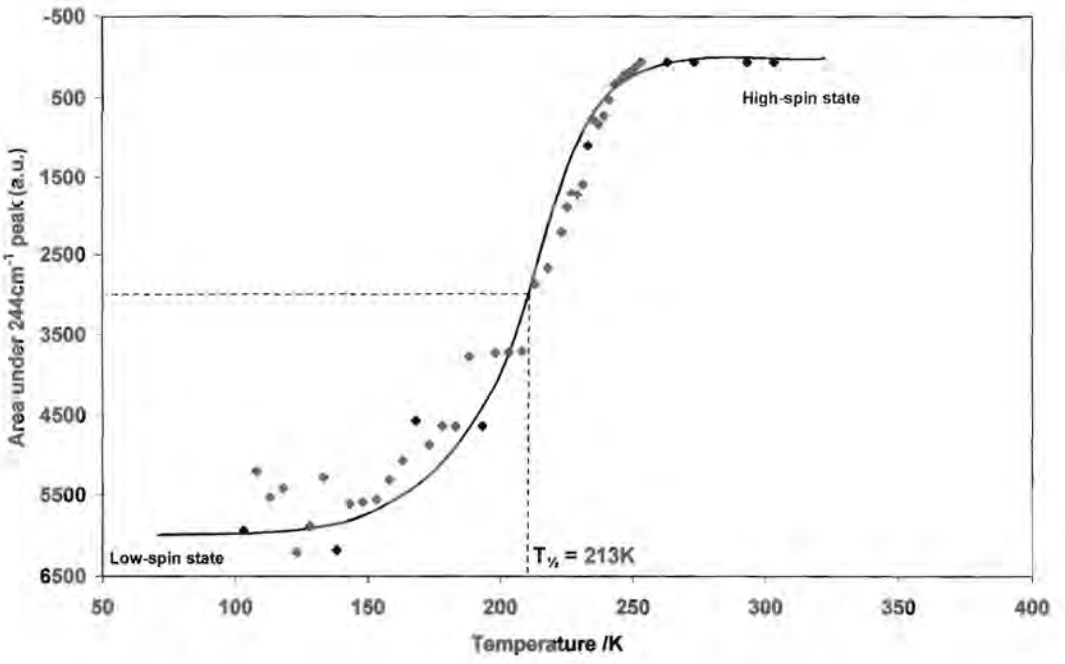

Figure 18 Transition curve obtained by plotting the intensity of the 244cm^{-1} peak (from **Figure 16**) as a function of temperature.

Chapter 6 – X-ray powder diffraction study: Results and Discussion

In this chapter the effects of proper drying and grinding of $[Fe(Htrz)_3](ClO_4)_2 \cdot 1.85H_2O$ specimens on the quality of X-ray powder patterns are reported and discussed.

6.1 Improvement of Crystallinity and Powder Patterns

Figure 19 shows that proper drying after the initial grinding increases the sample crystallinity and thereby the quality of the powder pattern. Pattern 1a is that of sample 4 directly after synthesis (note the amorphous region between 10° and 18° 2θ). 1b is the pattern of the same specimen after an additional 24 hours of drying (note the appearance of the peaks at ±11°, 12°, 16° and 18° 2θ). 1c shows the pattern of the specimen after 48 hours of drying and an additional 5 minutes of grinding.

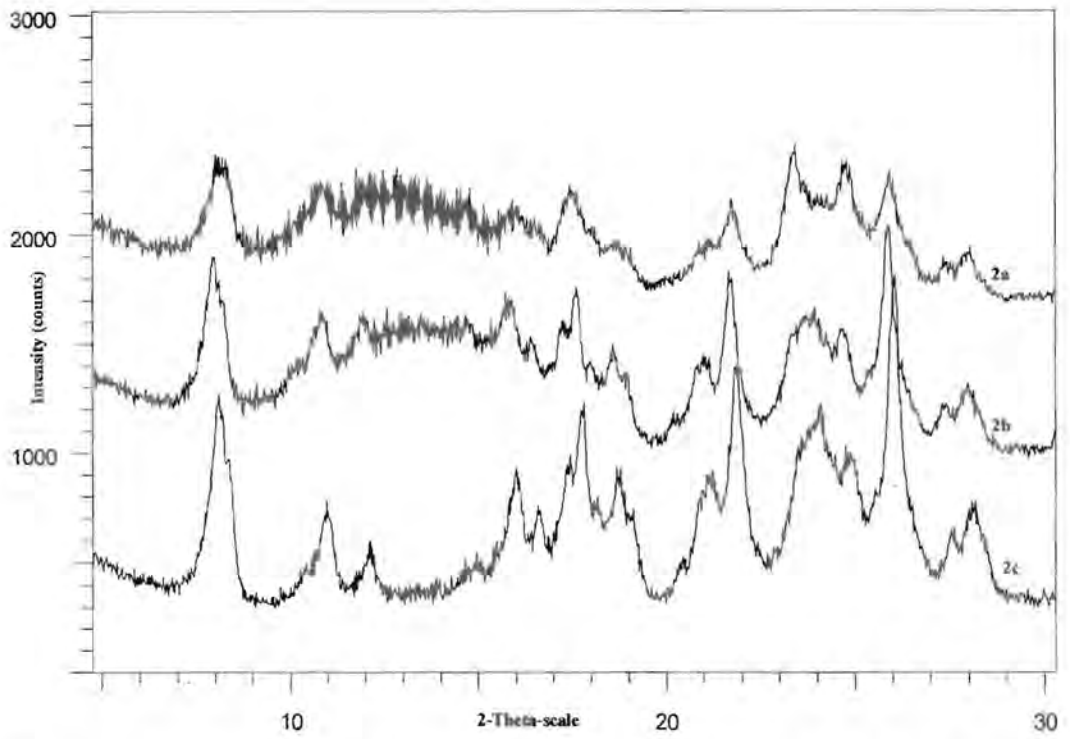

Figure 19 X-ray powder patterns of sample 4 showing that additional drying of the specimen increases crystallinity. (1a) No additional drying, (1b) 24h additional drying, (1c) 48h drying and 5 minutes grinding. [Pattern recording data: Range of 2θ: 3°-85° 2θ, step time: 3s]

6.2 Infrared Comparison of samples

Figure 20a and b show the mid- and far-infrared spectra of all four samples. In the mid-infrared spectra the absence of the Triazole ligand's R_8 ring torsion vibration (near 684cm^{-1}) and the presence of the 1215 cm^{-1} and 1305 cm^{-1} bands show that all four samples are the same compound with 1,2-bicoordinating Htrz-ligands[88]. In the far-infrared spectra, the position of the Fe-N stretching vibration at 300 cm^{-1} shows that all four compounds are in the low spin state at room temperature. The spectrum of sample 1 in the high spin state is given for comparison. The broadening of the Fe-N bands in the spectra of sample 2, 3 and 4, compared to that of sample 1, is most probably caused by the difference in sample pellet preparation mentioned in the experimental section.

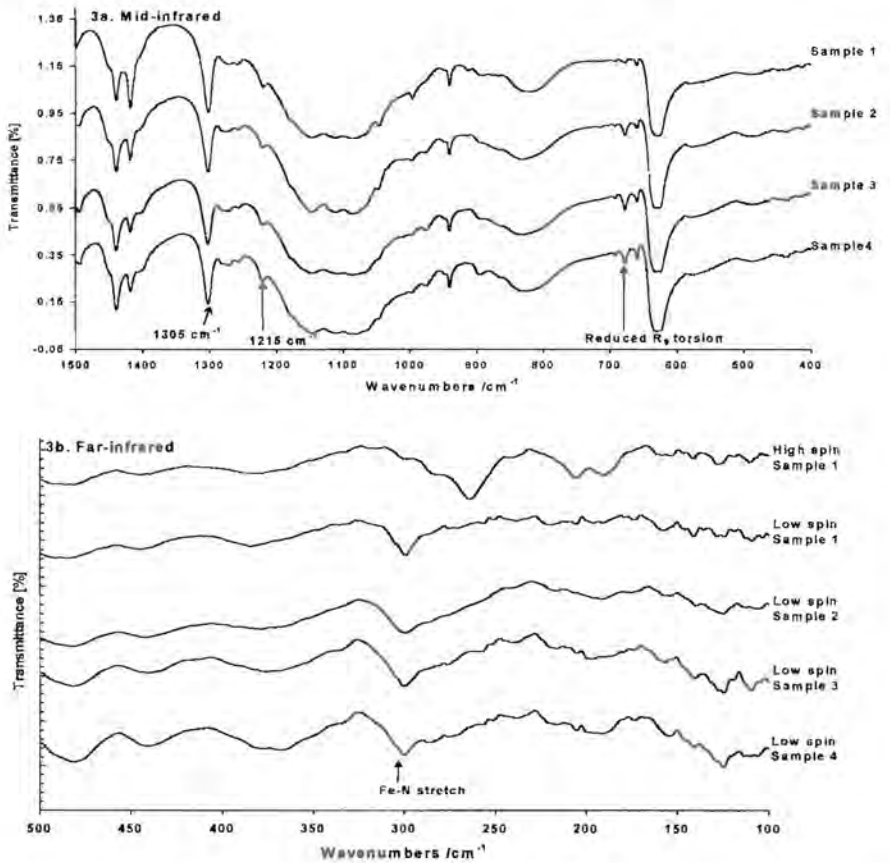

Figure 20 (a and b) Mid-infrared (Fig.20a) and Far-infrared (Fig.20b) spectra showing that all four samples are the same compound and in the low spin state at room temperature. The far-infrared spectrum of sample 1 in the high spin state is included for comparison.

6.3 Effects of preferential orientation on the powder patterns

In Figure 21 the X-ray powder diffraction patterns of sample 2 (21a), sample 3 (21b and 21c) and sample 1 (21d) are shown. As the infrared spectra in Figure 20 prove that all the samples are, in fact, the same compound, it is assumed that the differences between the powder patterns of the three compounds in Figure 21 can be attributed to preferential orientation effects. This assumption is supported by comparison of patterns 21a and 21b with patterns 21c and 21d. Note the high intensities of the peaks at 23.33° 2θ and 24.52° 2θ in 21a and 21b, as well as the presence of a small peak at 12.74° 2θ. Pattern 21c is of the same specimen as 21b, but with an additional 5 minutes of grinding. Here extra care was taken to avoid preferential orientation. After this additional treatment, the intensities of the two peaks at 23.33° 2θ and 24.52° 2θ are notably reduced and the peak at 12.74° 2θ has disappeared completely. Pattern 21c is thought to represent the true powder pattern of $[Fe(Htrz)_3](ClO_4)_2 \cdot 1.85H_2O$, as further grinding, drying and specimen surface correction, in addition to the treatment mentioned above, did not appear to lead to further improvement in the quality of the pattern.

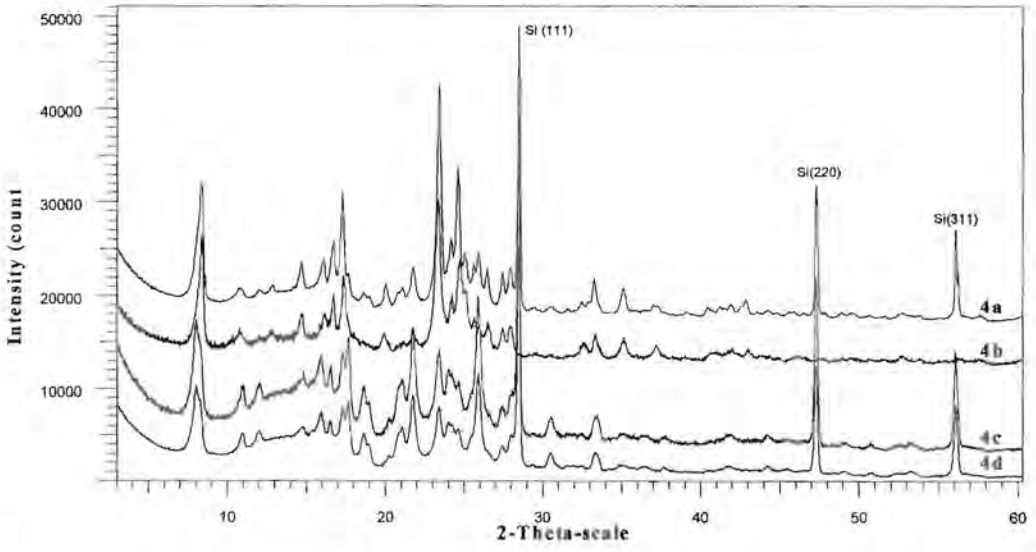

Figure 21 X-ray powder patterns of sample 2 (pattern 21a), sample 3 (21b and 21c) and sample 1 (21d) showing the effect of preferential orientation. Preferential orientation: 21a and 21b. No preferential orientation: 21c and 21d. [Pattern recording data: (21a, 21c and 21d) range of 2θ: 2.953°-64.960° 2θ, step time: 30s, Internal standard: Si(SRM640a). (21b) range of 2θ: 3°-85° 2θ, step time: 3s.]

6.4 Indexing of the powder pattern and comparison of structural data with $[Cu(Hyetrz)_3](ClO_4)_2 \cdot 3H_2O$

Preliminary indexing of the X-ray powder diffraction pattern 21c was performed by means of the computer program DICVOL[94]. 15 peak positions, with maximal absolute error of 0.04° 2θ, were used as input data (the peak at 10.798°2θ was not used). The peak positions were obtained after $K\alpha_2$-stripping using the software package *Diffrac plus, Eva version 3.0 from Bruker axs*. The only possible solution proposed by the DICVOL program was that of a cell with monoclinic symmetry. The calculated and observed peak positions, intensities and Miller indexes, as well as the calculated cell parameters and figures-of-merit are shown in Table 9 in Annex 6.

The cell parameters are compared to those of the Cu compound $[Cu(Hyetrz)_3](ClO_4)_2 \cdot 3H_2O$ where Hyetrz = 4-(2-hydroxyethyl)-1,2,4-triazole)[95] in Table 2 below and it shows similar framework-building $M(Ltrz_3)$ (M = Fe, Cu; L = H, C_2H_5O).

Table 2 Comparison of cell parameters of $[Fe(Htrz)_3](ClO_4)_2$ and $[Cu(Hyetrz)_3](ClO_4)_2 \cdot 3H_2O$.

	$[Fe(Htrz)_3](ClO_4)_2 \cdot 1.85H_2O$	$[Cu(Hyetrz)_3](ClO_4)_2 \cdot 3H_2O$
Cell parameters: in Å	c = 13.0321	a = 13.877(3)
	b = 20.6134	b = 23.023(5)
	a = 15.8160	c = 15.351(2)
β (°)	103.83	91.10(2)
Volume (Å^3)	4125.633	4904(2)
Space group	$P2_1/m$	$P2_1/n$

The parameter b = 23.023Å in the Cu compound decreases to 20.6125Å in the Fe compound because of the substitution of $-CH_2CH_2OH$ in the Cu compound with -H in the Fe compound (see Figure 22). The parameters a and c in the Cu compound are close to the c and a, respectively, of the Fe compound.

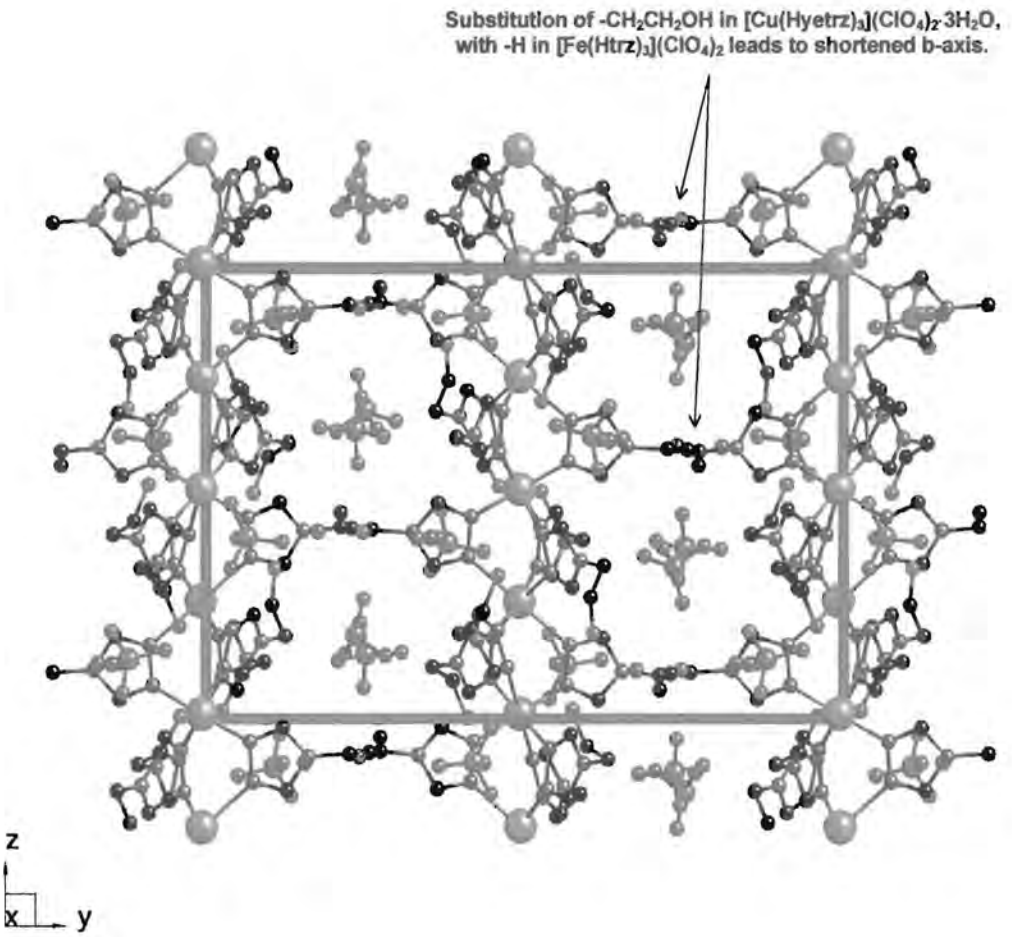

Figure 22 CRYSTAL MAKER ™ Drawing of the compound $Cu(Hyetrz)_3](ClO_4)_2 \cdot 3H_2O$ where Hyetrz = 4-(2-hydroxyethyl)-1,2,4-triazole) (Garcia et al. 1997). *Inorganic Chemistry*, 1997, 36, 6357-6365. Copyright 1997 American Chemical Society. Special thanks and acknowledgement to Y. Garcia for supplying the figure.

Chapter 7 – Conclusions and recommendations

As stated in Chapter 1, the aim of this research project was
to *study/review* the existing knowledge on spin-transition;
to *identify* unknowns or inconclusive theories about spin-transition polymers;
to *investigate* one or more of these unknowns in order to obtain a better understanding of spin-transition materials in general and polymeric spin-transition compounds in particular, and
to add to the pool of knowledge on the subject.

From the literature study/review it was determined that more information was required on the structural changes that occur in polymeric spin-transition compounds during spin-transition.

The infrared study showed that the Fe-N_6 coordination sphere has six equal Fe-N bonds in the low-spin state. It also showed that these Fe-N bonds weaken/lengthen during the spin-transition, with two of the bonds lengthening to a lesser degree than the other four. The pressure-dependent low-spin↔high-spin transition of $[Fe(Htrz)_3](ClO_4)_2$ was also discovered in the infrared study and a potential application of this is described in the box at the end of the chapter.

The Raman investigation showed that the Fe-N stretching mode that occurs in the region between 200 and 300 cm^{-1} in the Raman spectra of these compounds only appears in the low-spin state. The increasing intensity of this peak as a function of temperature, was directly related to the spin-transition phenomenon by deriving a spin-transition function curve from the peak intensity data. It could be concluded with a reasonable amount of certainty, that the appearance/disappearance of the peak was indicative of a change in the symmetry within the coordination sphere.

The initial aim of the X-ray powder diffraction study was to obtain a good quality, repeatable powder pattern for the compound, $[Fe(Htrz)_3](ClO_4)_2 \cdot 1.85H_2O$. This was

achieved for the compound in the low-spin state. From the results obtained, a procedure is suggested to obtain specimens of $[Fe(Htrz)_3](ClO_4)_2 \cdot 1.85H_2O$ that give reproducible, high-quality X-ray powder patterns:

1. After synthesis, the air-dried sample should be ground for ±5 minutes and then dried for an additional 24 to 48 hours. This is to eliminate any solvent that may be trapped within the powder. Improper drying of the sample leads to poor crystallinity and this in turn leads to a low-quality powder pattern with an amorphous region between 10° and 18° 2θ.
2. After proper drying, the sample should be ground for an additional 5 to 10 minutes after which other practical steps should be taken in order to avoid preferential orientation of the microcrystals (eg. sieving and surface correction with a razor blade).

Although the X-ray powder study did not focus on the *changes* that occur during spin-transition, a lot of useful information was obtained from the indexing of the powder data. It was determined that the low-spin compound has monoclinic symmetry, with cell parameters: a = 13.0321 Å, b = 20.6134 Å, c = 15.8160 Å, β = 103.83° and Volume = 4125.633 $Å^3$. These values were determined with figures of merit: M_{15} = 10.4 and F_{15} = 22.0 (0.0100, 68).

Recommendation

If additional studies were to be done on these compounds, it is suggested that attempts are made to obtain single crystals for the compound $[Fe(Htrz)_3]SO_4$. Although this compound does not undergo spin-transition, the infrared spectra show that it has a structure similar to $[Fe(Htrz)_3](ClO_4)_2$, and during this project a single crystal of $[Fe(Htrz)_3]SO_4$ was obtained. Unfortunately, the crystal was discarded at that time because it did not form part of the materials under study.

Potential application of spin-transition polymers in pressure sensors.

The figures below describe schematically how spin-transition compounds can be used in critical-pressure applications. In the first figure the pressure in the vacuum chamber is below the critical pressure, P_c, causing the spin-transition compound to turn white. The white surface reflects the laser light to the light detector, which can be connected to a computer or an alarm. In the second figure the pressure in the vacuum chamber is above the critical pressure, P_c, causing the spin-transition compound to turn purple. The purple surface will absorb the light or reflect it to a lesser degree, depending on the wavelength of the light used. The change in pressure can thus be observed at a critical point.

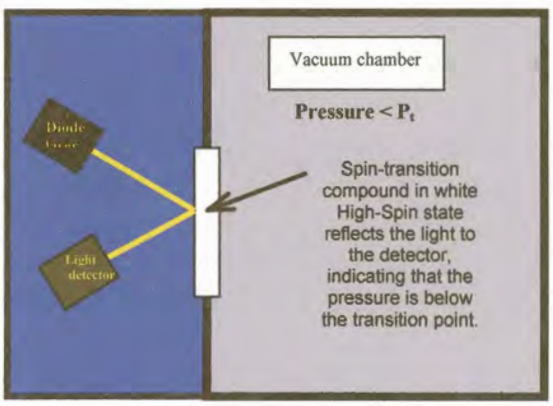

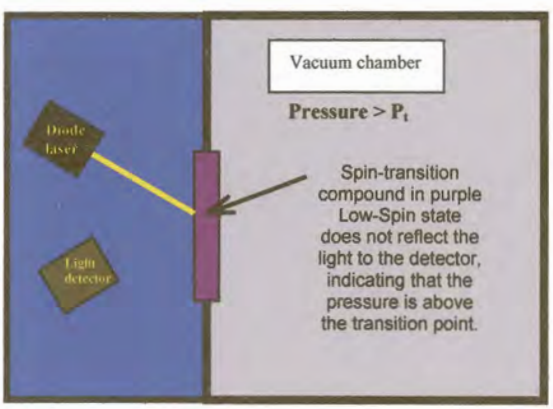

References

Note – Due to the fact that published studies on spin-transition often contain information obtained from more than one technique, some of the references have been grouped to simplify referencing in the main text. As a consequence of this, some duplicate inscriptions appear in the list below.

[1] "Promoting public understanding of Science and Technology in Southern Africa", Proceedings of a Southern African conference, Cape Town, Republic of South Africa, 4-7 December 1996, Edited by M. B. Ogunniyi, Published by the SSME, University of the Western Cape, **1997**.

[2] "South Africa's Green Paper on Science and Technology. *Preparing for the 21st Century.*", **1996**

[3] O. Kahn and C. J. Martinez, *Science*, **1998**, 279, 44.

Grouped References (UV-vis spectroscopy)

[4] G. Vos, R. A. le Fêbre, R. A. G. de Graaff, J. G. Haasnoot, and J. Reedijk, *J. Am. Chem. Soc.* **1983**, 105, 1682-1683.

[5] P. L. Franke, J. G. Haasnoot, and A. P. Zuur, *Inorganica Chimica Acta*, **1982**, 59, 5-9

Grouped References (magnetic susceptibility)

[6] J. Kröber, E. Codjovi, O. Kahn, F. Groliere and C. Jay, *J. Amer. Chem. Soc.* **1993**,115, 9810.

[7] O. Kahn, J. Kröber, C. Jay, *Adv. Mater.* **1992**; 4(11), 718.

[8] S. Decurtins, P. Gütlich, K. M. Hasselbach, A. Hauser, H. Spiering, *Inorg. Chem.*, **1985**, 24, 2174-2178

[9] J. Kröber, J. Audière, R. Claude, E. Codjovi, O. Kahn, J. G. Haasnoot, F Grolière, C. Jay, A. Bousseksou, J. Linarès, F. Varret and A. Gonthier-Vassal, *Chem. Mater.* **1994**, 6(8), 1404.

[10] W. Freugdenhil, J. H. van Diemen, R. A. G. de Graaf, J. G. Haasnoot, J. Reedijk, A. M. van der Kraan, O. Kanh, J. Zarembowitch, *Polyhedron*, **1990**, 9, 2971.

[11] B. Gallois, J-A. Real, C. Hauw, and J. Zarembowitch, *Inorg. Chem.*, **1990**, 29, 1152-1158.

[12] G. Vos, R. A. G. De Graaf, J. G. Haasnoot, A. M. Van der Kraan, P. De Vaal and J. Reedijk, *Inorg. Chem.* **1984**, 23, 2905.

[13] E. W. Müller, J. Ensling, H. Spiering and P. Gütlich, *Inorg. Chem.* **1983**, 22, 2074.

[14] M. Thomann, O. Kahn, J. Guilhem and F. Varret, *Inorg. Chem.* **1994**, 33, 6029.

[15] M. D. Timken, C. E. Strouse, S. M. Soltis, S. A. Daverio, D. N. Hendrickson, A. M. Abdel-Mawgoud, S. R. Wilson, *J. Am. Chem. Soc.*, **1986**, 108, 395-402.

[16] M. D. Timken, A. M. Abdel-Mawgoud and D. N. Hendrickson, *Inorg. Chem.* **1986**, 25,160.

[17] L. Wiehl, G. Kiel, C. P. Köhler, H. Spiering, and P. Gütlich, *Inorg. Chem.*, **1986**, 25, 1565-1571.

[18] S. Usha, R. Srinivasan and C.N.R. Rao, *Chemical Physics* **1985**, 100, 447.

[19] M. D. Timken, D. N. Hendrickson and E. Sinn, *Inorg. Chem.* **1985**, 24, 3947-3955.

[20] P. L. Franke, J. G. Haasnoot, and A. P. Zuur, *Inorganica Chimica Acta*, **1982**, 59, 5-9.

[21] W. Vreugdenhil, J. G. Haasnoot, O. Kahn, P. Thuèry, and J. Reedijk, *J. Am. Chem. Soc.*, **1987**, 109, 5272-5273.

[22] W. Vreugdenhil, S. Gorter, J. G. Haasnoot, and J. Reedijk, *Polyhedron*, **1985**, 4(10), 1769-1775.

[23] D. M. Halepoto, D. G. L. Holt, L. F. Larkworthy, G. J. Leigh, D. C. Povey, and G. W. Smith, *J. Chem. Soc. Chem. Commun.*, **1989**, 1322-1323.

Grouped References (Mössbauer spectroscopy)

[24] P. Gütlich, A. Hauser, H. Spiering, *Angew. Chem. Int. Ed. Engl.* **1994**, 33, 2024-2054.

[25] J. Kröber, J. Audière, R. Claude, E. Codjovi, O. Kahn, J. G. Haasnoot, F Grolière, C. Jay, A. Bousseksou, J. Linarès, F. Varret and A. Gonthier-Vassal, *Chem. Mater.* **1994**, 6(8), 1404.

[26] E. König, G. Ritter, S. K. Kulshreshtha, *Chem. Rev.* **1985**; 85: 219.

[27] G. Vos, R. A. le Fêbre, R. A. G. de Graaff, J. G. Haasnoot, and J. Reedijk, *J. Am. Chem. Soc.* **1983**, 105, 1682-1683.

[28] W. Freugdenhil, J. H. van Diemen, R. A. G. de Graaf, J. G. Haasnoot, J. Reedijk, A. M. van der Kraan, O. Kahn, J. Zarembowitch, *Polyhedron*, **1990**, 9, 2971.

[29] S. Decurtins, P. Gütlich, C. P. Köhler, and H. Spiering, *J. Chem. Soc. Chem. Commun.*, **1985**, 430-432.

[30] G. Vos, R. A. G. De Graaf, J. G. Haasnoot, A. M. Van der Kraan, P. De Vaal and J. Reedijk, *Inorg. Chem.* **1984**, 23, 2905.

[31] E. W. Müller, J. Ensling, H. Spiering and P. Gütlich, *Inorg. Chem.* **1983**, 22, 2074.

[32] M. Thomann, O. Kahn, J. Guilhem and F. Varret, *Inorg. Chem.* **1994**, 33, 6029.

[33] M. D. Timken, C. E. Strouse, S. M. Soltis, S. A. Daverio, D. N. Hendrickson, A. M. Abdel-Mawgoud, S. R. Wilson, *J. Am. Chem. Soc.*, **1986**, 108, 395-402.

[34] M. D. Timken, A. M. Abdel-Mawgoud and D. N. Hendrickson, *Inorg. Chem.* **1986**, 25,160.

[35] L. Wiehl, G. Kiel, C. P. Köhler, H. Spiering, and P. Gütlich, *Inorg. Chem.*, **1986**, 25, 1565-1571.

[36] M. D. Timken, D. N. Hendrickson and E. Sinn, *Inorg. Chem.* **1985**, 24, 3947-3955.

[37] J. Pebler, *Inorg. Chem.* **1983**, 22, 4125.

[38] M. Sorai, J. Ensling and P. Gütlich, *Chem. Phys.* **1976**, 18, 199.

Grouped References (EPR spectroscopy)

[39] W. Freugdenhil, J. H. van Diemen, R. A. G. de Graaf, J. G. Haasnoot, J. Reedijk, A. M. van der Kraan, O. Kanh, J. Zarembowitch, *Polyhedron*, **1990**, 9, 2971.

[40] M. D. Timken, D. N. Hendrickson and E. Sinn, *Inorg. Chem.* **1985**, 24, 3947-3955.

Grouped references (Single crystal X-ray diffraction)

[41] W. Freugdenhil, J. H. van Diemen, R. A. G. de Graaf, J. G. Haasnoot, J. Reedijk, A. M. van der Kraan, O. Kanh, J. Zarembowitch, *Polyhedron*, **1990**, 9, 2971.

[42] B. Gallois, J-A. Real, C. Hauw, and J. Zarembowitch, *Inorg. Chem.*, **1990**, 29, 1152-1158.

[43] G. Vos, R. A. G. De Graaf, J. G. Haasnoot, A. M. Van der Kraan, P. De Vaal and J. Reedijk, *Inorg. Chem.* **1984**, 23, 2905.

[44] M. Thomann, O. Kahn, J. Guilhem and F. Varret, *Inorg. Chem.* **1994**, 33, 6029.

[45] M. D. Timken, C. E. Strouse, S. M. Soltis, S. A. Daverio, D. N. Hendrickson, A. M. Abdel-Mawgoud, S. R. Wilson, *J. Am. Chem. Soc.*, **1986**, 108, 395-402.

[46] M. D. Timken, A. M. Abdel-Mawgoud and D. N. Hendrickson, *Inorg. Chem.* **1986**, 25,160.

[47] L. Wiehl, G. Kiel, C. P. Köhler, H. Spiering, and P. Gütlich, *Inorg. Chem.*, **1986**, 25, 1565-1571.

[48] M. D. Timken, D. N. Hendrickson and E. Sinn, *Inorg. Chem.* **1985**, 24, 3947-3955.

[49] W. Vreugdenhil, S. Gorter, J. G. Haasnoot, and J. Reedijk, *Polyhedron*, **1985**, 4(10), 1769-1775.

[50] D. M. Halepoto, D. G. L. Holt, L. F. Larkworthy, G. J. Leigh, D. C. Povey, and G. W. Smith, *J. Chem. Soc. Chem. Commun.*, **1989**, 1322-1323.

Grouped References (Powder X-ray diffraction)

[51] J. Kröber, J. Audière, R. Claude, E. Codjovi, O. Kahn, J. G. Haasnoot, F Grolière, C. Jay, A. Bousseksou, J. Linarès, F. Varret and A. Gonthier-Vassal, *Chem. Mater.* **1994,** 6(8), 1404.

[52] E. König, G. Ritter, S. K. Kulshreshtha, *Chem. Rev.* **1985**, 85, 219.

Grouped References (Infrared Spectroscopy)

[53] E. W. Müller, J. Ensling, H. Spiering and P. Gütlich, *Inorg. Chem.* **1983**, 22, 2074.

[54] J. H. Takemoto and B. Hutchinson, *Inorg. Chem.* **1973**, 12(3), 705.

[55] Y. Saito, J. Takemoto, B. Hutchinson and K. Nakamoto, *Inorg. Chem.* **1972**, 11(9), 2003.

[56] E. König and K. Madeja, *Spectrochimica Acta*, **1967**, 23A, 45.

[57] J. Pebler, *Inorg. Chem.* **1983**, 22, 4125.

[58] D. M. Adams, G. J. Long and A. D. Williams, *Inorg. Chem.* **1982**, 21,1049.

[59] P. L. Franke, J. G. Haasnoot, and A. P. Zuur, *Inorganica Chimica Acta*, **1982**, 59, 5-9.

[60] J. H. Takemoto, B. Streusand, and B. Hutchinson, *Spectrochimica Acta* A, **1974**, 30,827.

Grouped References (Raman Spectroscopy)

[61] J. Teraoka, S. Hashimoto, H. Sugimoto, M. Mori, and T. Kitagawa, *J. Am. Chem. Soc.*, **1987**, 109, 180-184.

[62] L. A. Lipscomb, B. Lee, and N. Yu, *Inorg. Chem.*, **1993**, 32, 281-286.

[63] S. Takahashi, J. W. Sam, J. Peisach, and D. L. Rousseau, *J. Am. Chem. Soc.*, **1994**, 116, 4408-4413.

[64] W. Wagner, and K. Nakamoto, *J. Am. Chem. Soc.*, **1989,** 111, 1590-1598.

[65] P. S. Rao, P. Ganguli, and B. R. McGarvey, *Inorg. Chem.*, **1981**, 20, 3682-3688.

[66] A. Michalovicz, J. Moscovici, B. Ducourant, D. Cracco, and O. Kahn, *Chem. Mater.*, **1995**, 7, 1833.

[67] A. Michalovicz, J. Moscovici, and O. Kahn, *J. Phys. IV (Paris)*, **1997**, C2-633.

[68] P. Gütlich, A. Hauser, and H. Spiering, *Angew. Chem. Int. Ed. Engl.*, **1994**, 33, 2024-2054.

[69] Tanabe-Sugano Diagrams, pp 453-458, "Concepts and Models of Inorganic Chemistry", 3rd ed., B Douglas, D McDaniel and J Alexander, John Wiley & Sons, Inc., **1994**

[70] O. Kahn, *Molecular Magnetism*, VCH, New York, **1993**.

[71] P. Gütlich, in *Mössbauer Spectroscopy Applied to Inorganic Chemistry, Vol.1* (Ed.: G. J. Long), Modern Inorganic Chemistry Series, Plenum Press, New York, **1984**.

[72] Physical Chemistry, 5th ed., PW Atkins, Oxford University Press ,**1994**.

[73] J. Zarembowitch, O. Kahn, *New J. Chem.* **1991**, 15, 181.

[74] M. Sorai, S. Seki, *J. Phys. Chem. Solids*, **1974**, 35, 555-570.

[75] G. A. Renovitch, W. A. Baker, Jr., *J. Am. Chem. Soc.*, **1967**, 89:24, 6377.

[76] Y. Garcia, P. J. Van Koningsbruggen, E. Codjovi, R. Lapouyade, O. Kahn, L. Rabardel, *J. Mater. Chem.* **1997**; 7(6): 857.

[77] D. W. Engelfriet, G. C. Verschoor, *Acta Crystallogr.*, **1982**, B37, 327.

[78] L. G. Lavrenova, V. N. Ikorskii V. A. Varnek, I. M. Oglezneva and S. V. Larionov, *Russian Journal of Coordination Chemistry*, **1990**, 16(5), 654.

[79] Y. Garcia, P. J. Van Koningsbruggen, R. Lapouyade, L. Fournès, L. Rabardel, O. Kahn, V. Ksenofontov, G. Levchenko, and P. Gütlich, *Chem. Mater.*, **1998**, 10, 2426-2433.

[80] J. G. Vos, *Inorganica Chimica Acta*, **1985**, 99, 117.

[81] E. König, K. Madeja and K. J. Watson, *J. Am. Chem. Soc.* **1968**, 90, 1146.

[82] B. Hutchinson, J. Takemoto and K. Nakamoto, *J. Am. Chem. Soc.* **1970**, 92, 3335.

[83] J. G. Haasnoot, (**1996**). "1,2,4-Triazoles As Ligands For Iron(Ii) High Spin ↔ Low Spin Crossovers", *O. Kahn (ed.), Magnetism: A Supramolecular Function* (Kluwer Academic Publishers, Netherlands), pp. 299-321.

[84] D. Bougeard, N. Le Calvé, B. Saint Roch and A. Novak, *J. Chem. Phys.* **1976**, 64(12), 5152.

[85] J. A. Faniran and J. E. Bertie, *J. Chem. Soc., Faraday Trans.* 2, **1977**, 73(9), 1272.

[86] *Spectral Atlas Computer Program (Demo Version), based on The Handbook of Infrared and Raman Spectra of Inorganic Compounds and Organic Salts*; R. A. Nyquist, R. O. Kagel, C. L. Putzig, M. A. Leugers, Academic Press.

[87] B. Hutchinson, J. Takemoto and K. Nakamoto, *J. Am. Chem. Soc.* **1970**, 92, 3335.

[88] J. G. Haasnoot, G. Vos and W. L. Groeneveld, *Z. Naturforsch.*, **1977**, 32b, 12, 1421.

[89] L. G. Lavrenova, V. N. Ikorskii, V. A. Varnek, I. M. Oglezneva and S. V. Larionov, *Russian Journal of Coordination Chemistry*, **1986**, 12(2), 207.

[90] G. J. Long and B. B. Hutchinson, *Inorg. Chem.* **1987**, 26(4), 609.

[91] J. K. McCusker, M. Zvagulis, H. G. Drickamer and D. N. Hendrickson, *Inorg. Chem.* **1989**, 28(7), 1380.

[92] L. Wiehl, G. Kiel, C. P. Köhler, H. Spiering, and P. Gütlich, *Inorg. Chem.*, **1986**, 25, 1565-1571.

[93] A. E. Kerr, Nai-Teng Yu, K. Gersonde, D. W. Parish, K. M. Smith. *J. Biol. Chem.* **1985**; 260(23): 12665.

[94] A. Boultif, and D. Louër, *J. Appl. Cryst.* **1991**, 24, 987-993.

[95] Y. Garcia, P. J. Van Koningsbruggen, G. Bravic, P. Guionneau, D. Chasseau, G. L. Cascarano, J. Moscovici, K. Lambert, A. Michalowicz, and O. Kahn, *Inorganic Chemistry,* **1997**, 36, 6357-6365.

Annex 1 – Magnetochemical measurements

The values that are measured with the Gouy-balance are gram susceptibility, χ. A more useful value in chemistry is the molar susceptibility, χ_m, which is obtained by multiplying χ and the molar mass of the substance.

$$\chi_m = \chi \cdot M$$

Since the molar mass of the polymeric structures investigated here was not determined, the value of M was taken as the mass of the monomeric units that make up the polymer, i.e.

M = mass of metal ion + mass of ligands + mass of counter anions.

If χ_m is positive, the compound is paramagnetic, and if it is negative χ_m is negative. χ_m is described by the formula:

$$\chi_m(complex) = \chi_m^{'}(metal\ \ ion) + \chi_m(ligands) + \chi_m(counter\ \ ions)$$

It is necessary to correct for the diamagnetism of the other groups and therefore the main interest is in $\chi_m^{'}$. The diamagnetic corrections that were used are given in Table 3.

Table 3 Diamagnetic corrections used in the Magnetic susceptibility calculations

Species	**Diamagnetic Correction** $\times 10^{-8}$ **g^{-1}.atom^{-1}**
1H-1,2,4-Triazole	35
4-NH_2-1,2,4-Triazole	43
Cl^-	23.4
ClO_4^-	32
SO_4^{2-}	40.1

The effective magnetic moment, μ_{eff}, is obtained from the equation:

$$\mu_{eff} = 2.83\sqrt{\chi_m' T}$$

with T = temperature in Kelvin and μ_{eff} in Bohr magnetons.

The number of unpaired electrons are then obtained from:

$$\mu_{eff} = \sqrt{n(n+2)}$$

The following mass measurements have to be made:

- mass of the empty tube, without the magnetic field, w_1
- mass of the empty tube in the magnetic field, w_2
- mass of the tube, filled to the mark with water, without the magnetic field, w_3
- mass of the tube, filled with the finely powdered complex, without the magnetic field, w_4
- mass of the tube, filled with the finely powdered complex, with the magnetic field on, w_5

The following relations can then be used:

$\Delta_w = (w_5 - w_4) - (w_2 - w_1)$

$V = (w_3 - w_1)/\rho(H_2O)$ $\quad (\rho(H_2O) = 0.998\ g/cm^3)$

$\chi_o = 0.36 \times 10^{-6}$ $\quad$ (Paramagnetic oxygen is displaced by the sample)

$m = w_4 - w_1$

A standard with known magnetic moment is then used to calibrate the Gouy balance in order to use the relation:

$$\chi_s' = (a\Delta_w + \chi_o)V/m$$

A calibration constant, a, is obtained.

$\chi_s'([Ni(en)_3]S_2O_3) = 11.04 \times 10^{-6}$ (20°C)

$[Ni(en)_3]S_2O_3$ can be prepared with a high degree of purity. It is not hygroscopic, it is stable and gives good packing in the tube. The compound obeys the Curie-Weiss law with $q = 43°$.

Measurements of the susceptibilities, of all four the studied compounds at room temperature, gave the following results:

Purple $[Fe(Htrz)_3](ClO_4)_2$ (suspected low-spin):
$0.39 \approx$ **0 unpaired electrons** (i.e. Low-spin)

White $[Fe(NH_2trz)_3](ClO_4)_2$ (suspected high-spin):
$3.74 \approx$ **4 unpaired electrons** (i.e. High-spin)

Purplish-brown $[Fe(Htrz)_3]Cl_2$ (suspected low-spin):
$0.995 \approx$ **1 unpaired electron**
(i.e. mixed state with majority of the Fe-centres Low-spin)
(Since the complex is supposed to be d^6, this result is taken to imply that some of the Fe^{2+} has oxidised to Fe^{3+}, indicated by the browning of the purple sample)

White $[Fe(Htrz)_3]SO_4$ (suspected high-spin):
$4.066 \approx$ **4 unpaired electrons** (i.e. High-spin)

Annex 2 - Results from elemental analysis of the four samples used in the XRD study.

Table 4 Elemental analysis of sample 1 to 4 and theoretical mass percentages of two possible forms of the compound.

	Sample age at the start of the study.	**Fe(%)**	**C(%)**	**N(%)**	**H(%)**
Sample 1	1 day	9.64	14.45	24.53	2.49
Sample 2	1 week	9.85	15.11	25.45	2.64
Sample 3	15 months	9.51	15.14	25.62	2.51
Sample 4	2 hours	9.47	14.99	24.97	2.68
Theoretical calculation for $[Fe(Htrz)_3](ClO_4)_2 \cdot 1.85H_2O$		11.28	14.55	25.45	2.58
Theoretical calculation for $[Fe(Htrz)_3](ClO_4)_2$		12.09	15.60	27.28	1.96

The difference between the expected and found values of Fe is assumed to be due to insufficient sensitivity of the analysis technique. The stoichiometry of the four different samples indicate a partially hydrated compound with a proper formula: $[Fe(Htrz)_3](ClO_4)_2 \cdot 1.85H_2O$.

Annex 3 – Instrument and Data collection parameters for Powder Diffraction Analysis

Table 5 Instrument and data collection parameters for X-ray powder diffraction analysis

Instrument	Siemens D-501
Radiation	Cu *Kα* (1.5418 Å)
Temperature	25°C
Specimen	flat-plate, rotating (30 RPM)
Power Setting	40 kV, 40 mA
Soller slits	2° (diffracted beam side)
Divergence slits	1°
Receiving slits	0.05°
Monochromator	Secondary, graphite
Detector	scintillation counter
Step width	0.02° 2θ

Annex 4 – Mid-infrared frequencies of Htrz, $[Fe(Htrz)_3](ClO_4)_2$ and $[Fe(Htrz)_3]Cl_2$

Table 6 Comparison of the mid-infrared frequencies of the free Htrz ligand, $[Fe(Htrz)_3](ClO_4)_2$ and $[Fe(Htrz)_3]Cl_2$. * Centre of gravity of band ** Several broad bands

Frequencies / cm^{-1}				Assignment
Published [84]	Observed			
Htrz	Htrz	$[Fe(Htrz)_3](ClO_4)_2$	$[Fe(Htrz)_3]Cl_2$	
3124s, 3116s	3131s, 3121s, 3114s	3085s, 3050s	3090s, 3045s	CH stretch
2730vs*	2853s*	2985-2409**	2978-2570**	NH stretch
1830m, 1547m	1766m, 1545m	1809w, 1536m	-	combination
1535m	1532m	1513m	1513s	R_1 ring stretch
1488vs	1485s	1419m	1419s	R_2 ring stretch
1383m	1380m	-	-	R_3 ring stretch
-	-	1300m	1301s	R_3 ring stretch / CH bend
1364w, 1304w	1362w, 1302w	-	-	Combination
1272vs	1273s	-	-	CH bend
1260vs	1257s	-	1220m	R_4 ring stretch
1184m	1180m	-	-	NH bend
-	-	1050-1170bs	-	ClO_4
1146s	1147s	1146s	1147s	R_5 ring breathing
1058m	1057m	1046s	1049s	CH bend
982vs	980s	996m	996m	R_6 ring bend
968m 957m 950m	956m	914w	-	R_7 ring bend
943m 934m	930m	-	950w	NH out-of-plane
-	-	935m	-	ClO_4
892m, 885m	884s	824m	858bm, 833bm	CH out-of-plane
684m 680m	683s	-	677vs	R_8 ring torsion
652m	649s	-	634vs	R_9 ring torsion
-		630, 460 vw		ClO_4

Annex 5 – Low-frequency Raman bands of the complexes and their pure starting materials

Table 7 Recorded low-frequency Raman bands (in cm^{-1}) of $[Fe(NH_2trz)_3](ClO_4)_2$ and its pure starting materials.

Pure NH_2trz	Pure $Fe(ClO_4)_2$	$[Fe(NH_2trz)_3](ClO_4)_2$ Complex		Tentative Assignment
		Low-spin state (158K)	High-spin state (249K)	
55		60	~60	Lattice modes
67		75	75	
102				
		115	115	
			124	
131		136	131	
153				
162				
173			172	
			180	
		198		
	464	458	458	$\nu_2(E)$ (ClO_4^-)[86]
	627	621+633	625	$\nu_4(F_2)$ (ClO_4^-)[86]

Table 8 Low-frequency Raman bands (in cm^{-1}) of the three Htrz-containing complexes and their pure starting materials. (sh = shoulder, b = broad)

Pure Htrz from literature[84,85]		Pure Htrz Observed	Pure $Fe(ClO_4)_2$ salt	$[Fe(Htrz)_3](ClO_4)_2$ complex		$[Fe(Htrz)_3]Cl_2$	$FeSO_4$ salt	$[Fe(Htrz)_3]SO_4$
Raman Frequency	Description			low-spin (77K)	high-spin (298K)	low-spin		high-spin
					41			
54	Interchain	50		54		50		50 sh
55	Interchain							
58	NH-N Bend	58						
61	NH-N Bend				61			
65				67-69		64		65 sh
71	NH-N Bend	76			73			70-75 vs
83	Chain torsion							
86	Chain torsion			87				89 sh
105	NH-N Bend				99			~108
117	NH-N Bend	118			112	120 sh, b		114
128	NH-N Bend			126	126	126 sh, b		
131	NH-N Bend			130	134			
				140		142 sh, b		140
155		157			152	150 sh, b		158
162	NH-N Bend							162
176	Interchain							
199	NH-N stretch				199	197 vs		188
200	Combination							
200	NH-N stretch			201				
	$\nu_2(E)$ (ClO_4^-/SO_4^{2-} anion)		464	458	465		450	450
	$\nu_4(F_2)$ (ClO_4^-/SO_4^{2-} anion)		627	624	623		620	606+623

Annex 6 – Powder Diffraction Data

Table 9 X-ray powder diffraction data and calculated cell parameters for sample 3 of the compound $[Fe(Htrz)_3](ClO_4)_2 \cdot 1.85H_2O$

$2\theta_{calc}$(°)	$2\theta_{obs}$(°)	d_{calc} (Å)	d_{obs} (Å)	I/I_o	(hkl)
7.920	7.941	11.163	11.125	61	$10\bar{1}$
8.200	8.188	10.784	10.789	56	011
10.940	(10.798)	8.085	(8.187)	27	111
11.970	11.948	7.395	7.401	22	$20\bar{1}$
14.640	14.640	6.049	6.046	30	012
14.670		6.038			031
15.880	15.857	5.581	5.584	46	$20\bar{2}$
16.440	16.464	5.392	5.380	37	$02\bar{2}$
16.450		5.387			$21\bar{2}$
17.180	17.197	5.161	5.152	60	221
17.210		5.153			040
17.600	17.591	5.039	5.038	56	$31\bar{1}$
17.620		5.034			$23\bar{1}$
18.520	18.538	4.792	4.782	30	122
18.590		4.773			041
18.920	18.918	4.689	4.687	20	$13\bar{2}$
18.970		4.679			$14\bar{1}$
19.360	19.346	4.585	4.584	5	320
20.200	20.178	4.395	4.397	16	202
20.210		4.395			301
20.760	20.741	4.279	4.279	26	240
20.890	20.875	4.252	4.252	28	132
20.910		4.248			$11\bar{3}$

$2\theta_{calc}$(°)	$2\theta_{obs}$(°)	d_{calc} (Å)	d_{obs} (Å)	I/I_o	(hkl)
21.010	20.988	4.228	4.229	32	$24\bar{1}$
21.060		4.218			003
21.650	21.677	4.105	4.096	71	330
22.810	22.855	3.899	3.888	22	241
22.950		3.875			$41\bar{1}$
23.460	23.361	3.792	3.805	86	$33\bar{2}$
23.500		3.786			$24\bar{2}$
23.910	23.912	3.721	3.718	52	$30\bar{3}$
24.040		3.702			232
24.040		3.702			331
24.070	24.115	3.698	3.688	55	$40\bar{2}$
24.150		3.685			$42\bar{1}$
24.510	24.523	3.632	3.627	57	250
24.510		3.632			340
24.720		3.601			$25\bar{1}$
25.810	25.855	3.452	3.443	100	401
25.930		3.436			060
26.880	26.882	3.316	3.314	19	$25\bar{2}$
26.890		3.316			061
27.390	27.368	3.256	3.256	24	$10\bar{4}$
27.390		3.256			$43\bar{2}$
27.420		3.253			$40\bar{3}$
27.830	27.916	3.205	3.193	34	223
27.880		3.200			161
28.650	28.659	3.116	3.112	12	$26\bar{1}$
28.750		3.105			$12\bar{4}$
29.240	29.253	3.054	3.050	4	$35\bar{2}$

$2\theta_{calc}$(°)	$2\theta_{obs}$(°)	d_{calc} (Å)	d_{obs} (Å)	I/I_o	(hkl)
29.400		3.038			510
30.400	30.450	2.940	2.933	16	$43\bar{3}$
30.420		2.939			$52\bar{2}$
30.490		2.932			114
30.920	30.931	2.892	2.889	4	170
31.120		2.874			034
31.130		2.873			$53\bar{1}$
31.570	31.617	2.834	2.828	6	501
31.670		2.825			$50\bar{3}$
31.710		2.822			243
32.370	32.405	2.765	2.761	8	$41\bar{4}$
32.410		2.762			$35\bar{3}$
33.260	33.321	2.694	2.687	21	$42\bar{4}$
33.390		2.683			214
34.800	34.822	2.578	2.574	6	$61\bar{2}$
34.820		2.577			080
34.840		2.575			$21\bar{5}$
35.120	35.115	2.555	2.554	7	$15\bar{4}$
35.140		2.554			$45\bar{3}$
36.560	36.549	2.458	2.457	7	025
36.620		2.454			$44\bar{4}$
37.690	37.717	2.386	2.383	6	082
37.740		2.384			611
38.100	38.129	2.362	2.358	4	$46\bar{3}$
38.130		2.360			$47\bar{1}$
40.460	40.424	2.229	2.230	4	363
40.480		2.228			513

$2\theta_{calc}$(°)	$2\theta_{obs}$(°)	d_{calc} (Å)	d_{obs} (Å)	I/I_o	(hkl)
41.630	41.706	2.169	2.164	8	$27\bar{4}$
41.700		2.166			$46\bar{4}$
41.940	41.908	2.154	2.154	9	$55\bar{4}$
41.950		2.154			092
42.870	42.842	2.109	2.109	6	192
42.880		2.109			006
44.230	44.232	2.047	2.046	9	283
44.260		2.046			$70\bar{4}$
45.530	45.520	1.992	1.991	5	$14\bar{6}$
45.560		1.991			2 10 0
46.520	46.497	1.952	1.952	5	046
46.530		1.952			623
47.730	47.690	1.905	1.905	4	415
47.770		1.904			$58\bar{3}$
48.420	48.412	1.880	1.879	3	$76\bar{2}$
48.480		1.878			056
49.110	49.092	1.855	1.854	4	$59\bar{1}$
49.120		1.855			643
49.130		1.854			$21\bar{7}$
50.750	50.747	1.799	1.798	4	1 11 $\bar{2}$
50.790		1.797			066
50.800		1.797			316
52.630	52.603	1.739	1.739	4	$14\bar{7}$
52.690		1.737			$81\bar{5}$
53.260	53.242	1.720	1.719	6	812
53.300		1.719			$82\bar{5}$

$2\theta_{calc}$(°)	$2\theta_{obs}$(°)	d_{calc} (Å)	d_{obs} (Å)	I/I_o	(hkl)
55.030	54.999	1.669	1.668	2	176
55.080		1.667			217
56.630	56.598	1.625	1.625	5	237
56.650		1.625			$30\bar{8}$
58.590	58.559	1.575	1.575	1	$29\bar{6}$
58.590		1.575			3 10 4
58.590		1.575			$79\bar{3}$

Cell parameters: Monoclinic system with a = 13.0321 Å, b = 20.6134 Å, c = 15.8160 Å, β = 103.83° and Volume = 4125.633 Å^3.

[M_{15} = 10.4] [F_{15} = 22.0 (0.0100, 68)]